

Neuropilin 1 mediates epicardial activation and revascularization in the regenerating zebrafish heart

Vanessa Lowe^{1,*}, Laura Wisniewski¹, Jacob Sayers¹, Ian Evans¹, Paul Frankel¹, Nadia Mercader-Huber², Ian C. Zachary^{1,‡} and Caroline Pellet-Many^{3,‡}

ABSTRACT

Unlike adult mammals, zebrafish can regenerate their heart. A key mechanism for regeneration is the activation of the epicardium, leading to the establishment of a supporting scaffold for new cardiomyocytes, angiogenesis and cytokine secretion. Neuropilins are co-receptors that mediate signaling of kinase receptors for cytokines with crucial roles in zebrafish heart regeneration. We investigated the role of neuropilins in response to cardiac injury and heart regeneration. All four neuropilin isoforms (*nrp1a*, *nrp1b*, *nrp2a* and *nrp2b*) were upregulated by the activated epicardium and an *nrp1a*-knockout mutant showed a significant delay in heart regeneration and displayed persistent collagen deposition. The regenerating hearts of *nrp1a* mutants were less vascularized, and epicardial-derived cell migration and re-expression of the developmental gene *wt1b* was impaired. Moreover, cryoinjury-induced activation and migration of epicardial cells in heart explants were reduced in *nrp1a* mutants. These results identify a key role for Nrp1 in zebrafish heart regeneration, mediated through epicardial activation, migration and revascularization.

KEY WORDS: Epicardium, Heart, Neuropilin, Regeneration, Zebrafish

INTRODUCTION

Ischemic heart disease remains the leading cause of death worldwide and, although improved therapeutic treatments have led to an increase in myocardial infarction (MI) survival rates (Cahill and Kharbada, 2017; Roger, 2013; von Gise et al., 2011), cardiac function often remains severely compromised because adult mammalian hearts replace damaged tissue with an irreversible fibrotic scar (Dobaczewski et al., 2010; Porrello et al., 2011). This often leads to the development of chronic heart failure, further MIs and fatal arrhythmias. In contrast to mammals, zebrafish have the remarkable ability to regenerate lost or damaged cardiac tissue via

cardiomyocyte proliferation and resorption of fibrotic tissue, ultimately restoring cardiac function (Chablais et al., 2011; González-Rosa et al., 2011; Jopling et al., 2010; Poss et al., 2002). Understanding the underlying mechanisms that govern zebrafish heart regeneration could identify therapeutic targets important for stimulating cardiac repair following MI in mammals.

Zebrafish heart regeneration involves a well-described, but incompletely understood, sequence of cellular processes and signaling events. The epicardium, a mesothelial cell monolayer encasing the heart, has been strongly implicated as a key regulator of the regenerative response (Cao and Poss, 2018; Masters and Riley, 2014; Zhou and Pu, 2011). Upon cardiac damage, the epicardium is activated (Schnabel et al., 2011; van Wijk et al., 2012), undergoing proliferation and secreting cytokines that stimulate cardiomyocyte cell cycle re-entry (Kikuchi et al., 2010). Autocrine and paracrine signals induce a subpopulation of epicardial cells to undergo a process known as epithelial to mesenchymal transition (EMT) (Kim et al., 2010; Lepilina et al., 2006). These epicardial cells adopt an embryonic-like gene expression profile, migrate into the injured region and differentiate into fibroblasts and mural cells that support revascularization (González-Rosa et al., 2012; Lepilina et al., 2006). Some of the signaling pathways required for the epicardial regenerative response in zebrafish have been identified and characterized. In particular, platelet-derived growth factor (PDGF)-BB and fibroblast growth factor (FGF) are both essential for epicardial EMT and coronary neovascularization in the regenerating zebrafish heart (González-Rosa et al., 2012; Kim et al., 2010; Lepilina et al., 2006). Vascular endothelial growth factor (VEGF) was also found to have a key role in the early revascularization of the injured area (Marín-Juez et al., 2016).

PDGF, FGF and VEGF are all ligands for neuropilin (NRP) transmembrane receptors (Ball et al., 2010; Pellet-Many et al., 2011; West et al., 2005). NRP1 and NRP2 share similar homology domain organization, with a large extracellular region essential for ligand binding, a single transmembrane domain and a short cytoplasmic domain (Pellet-Many et al., 2008). NRP1 was first identified as a regulator of angiogenesis and neurogenesis mediated via VEGF and semaphorin3A (Sema3aa), respectively (Gu et al., 2003; Kawasaki et al., 1999; Kitsukawa et al., 1997). In zebrafish, it is also required for vascular development and is a mediator of Vegf-dependent angiogenesis (Lee et al., 2002). Furthermore, NRPs have been shown to mediate signaling pathways for other cytokines, including PDGF, FGF and transforming growth factor (TGF)- β in various tissues in both physiological and pathological settings (Glinka and Prud'homme, 2008; Kofler and Simons, 2016; Pellet-Many et al., 2011; West et al., 2005). NRPs have also been reported to have a role in EMT in carcinomas (Adham et al., 2014; Chu et al., 2014; Grandclement et al., 2011); however, despite their known interactions with cytokines implicated in EMT, their role in the epicardial response and revascularization of the injured heart after

¹Centre for Cardiovascular Biology and Medicine, Division of Medicine, The Rayne Building, University College London, London WC1E 6JJ, UK.

²Department of Developmental Biology and Regeneration, Institut für Anatomie, Universität Bern, Baltzerstrasse 2, 3012 Bern, Switzerland. ³Department of Comparative Biomedical Sciences, Royal Veterinary College, Royal College Street, London NW1 0TU, UK.

*Present address: The William Harvey Research Institute, Translational Medicine and Therapeutics, Charterhouse Square, Barts and the London School of Medicine and Dentistry, Queen Mary University of London, London EC1M 6BQ, UK.

‡Authors for correspondence (c.pellet-many@ucl.ac.uk; i.zachary@ucl.ac.uk)

© P.F., 0000-0001-8820-5809; N.M.-H., 0000-0002-0905-6399; I.C.Z., 0000-0002-4464-3791; C.P.-M., 0000-0003-1894-3907

This is an Open Access article distributed under the terms of the Creative Commons Attribution License (<https://creativecommons.org/licenses/by/4.0>), which permits unrestricted use, distribution and reproduction in any medium provided that the original work is properly attributed.

cardiac damage is currently unknown. We used the zebrafish heart cryoinjury model (González-Rosa and Mercader, 2012) to investigate the spatiotemporal expression of the four zebrafish *nrp* isoforms (*nrp1a* and *nrp1b*, and *nrp2a* and *nrp2b*, orthologs of human *NRP1* and *NRP2*, respectively) in the regenerating heart. We show that all were upregulated in response to cryoinjury, with distinctive endocardial and epicardial expression during the regenerative response. NRPs are expressed in activated epicardial cells and, zebrafish expressing a truncated loss-of-function *Nrp1a* (*nrp1a^{sa1485}*) showed impaired epicardial response to injury, indicated by the downregulation of *WT1 transcription factor b* (*wt1b*; also known as *Wilms' tumor 1b*) expression. Epicardial explants from *nrp1a^{sa1485}* fish exhibited reduced epicardial cell migration compared with wild-type fish explants. Moreover, the revascularization of the injured area was also impaired in mutant fish. We also used a rat epicardial cell line (Wada et al., 2003) to investigate potential downstream targets of NRP1 and found that downregulating the expression of NRP1 via small hairpin (sh)RNA adenovirus infection, led to a decrease in β -catenin expression, which is an important regulator of EMT (Duan et al., 2012; von Gise et al., 2011; Zamora et al., 2007). These findings reveal an essential role for Nrps in zebrafish heart regeneration, mediated by a new function for *Nrp1a* in epicardial activation and cell movement.

RESULTS

Neuropilins are upregulated during zebrafish heart regeneration

We quantified *nrp1a*, *nrp1b*, *nrp2a* and *nrp2b* mRNA levels in whole ventricles following cardiac cryoinjury by absolute RT-quantitative (q)PCR and compared their expression with that in sham-operated hearts. *Nrp1a*, *nrp1b* and *nrp2a* were upregulated 3- to 5-fold in injured hearts compared with sham-operated hearts early during the regenerative process (1 and 3 days post cryoinjury, dpci) and returned to endogenous basal levels thereafter ($P=0.0019$ and $P<0.0001$ for *nrp1a* at 1 dpci and 3 dpci, respectively; $P=0.0007$ for *nrp1b* at 3 dpci and $P=0.0051$ and $P<0.0001$ for *nrp2a* at 1 dpci and 3 dpci, respectively) (Fig. 1A). In line with a previous publication (Martyn and Schulte-Merker, 2004), *nrp2b* was the most highly expressed isoform in the heart under control conditions (Fig. 1A). However, qPCR did not show any significant *nrp2b* changes following cardiac damage, probably because any localized or cell type-specific cardiac upregulation of this isoform was masked by its high basal expression.

We also analyzed the expression of molecules implicated in Nrp-mediated signaling pathways and others with a known role in zebrafish heart regeneration (Fig. S1). Consistent with previous work, *pdgfrb*, *pdgfab* and *tgfb1a* were all upregulated early after cryoinjury (Fig. S1) (Chablais and Jazwinska, 2012; Lepilina et al., 2006). Given that NRPs are VEGF co-receptors, we examined the regulation of *vegfaa*, *vegfc* and the VEGF receptors *kinase insert domain receptor like (kdrl)* and *fms-related tyrosine kinase 1 (flt1)*. In accordance with previously published data (Lien et al., 2006), *vegfc* was significantly upregulated following cardiac cryoinjury (Fig. S1), but we could not detect any significant change in the expression of *vegfaa*, *kdrl* and *flt1*. In this context and at this time following the injury, *vegfc* is probably involved in inflammation and lymphangiogenesis, as previously reported (Vieira et al., 2018).

Nrp1 protein expression in zebrafish ventricles, detected by western blot, was observed as two bands of ~130 kDa and 150 kDa, corresponding to *Nrp1a* [916 amino acids (aa)] and *Nrp1b* (959 aa), respectively (Fig. 1B). From 3 dpci and later, immunoblotting revealed an upregulation of *Nrp1* proteins in the injured hearts

compared with sham-operated hearts, although this did not reach statistical significance (Fig. 1B).

Neuropilins are upregulated in the epicardium and the endocardium following cryoinjury

We used *in situ* hybridization to delineate the spatiotemporal expression of *nrp* family genes following cryoinjury (Fig. 1C). The specificity of the *nrp* RNA probes was initially analyzed in zebrafish embryos (Fig. S2), confirming expression patterns similar to previous observations in the literature (Martyn and Schulte-Merker, 2004; Yu et al., 2004). In control sham-operated adult zebrafish hearts, *nrp1a* was expressed by the epicardium and *nrp2b* was widely expressed by the myocardium (Fig. 1C). *In situ* hybridization revealed mRNA upregulation of all neuropilin isoforms in the epicardium and at the interface between the healthy myocardium and the injured tissue at 1 dpci. At 3 dpci, both *nrp1a* and *nrp2a* were strongly and more widely upregulated by the activated epicardium, whereas *nrp1b* was expressed at the injury border. At 14 dpci, strong expression of *nrp1a* persisted in the epicardium adjacent to the injured area, and *nrp1b* was localized in the epicardium and the endocardium contiguous to the injured area. By 60 dpci, when heart regeneration was largely complete, expression of all *nrp* isoforms had returned to basal expression levels, which correlated with the gene expression data (data not shown).

To identify the *Nrp1*-expressing cells within the regenerating heart, we used co-immunofluorescent staining with specific endothelial, myocardial and epicardial markers. In *tg(fli1a:EGFP)^{v1}* zebrafish, in which EGFP is specifically expressed in vascular endothelial cells, *Nrp1* was co-expressed by *fli1a*-EGFP-expressing cells in sham hearts, consistent with expression of *Nrp1* by coronary vessels and endocardium (Fig. 2A, upper row). *Nrp1* expression was also evident in *fli1a*-EGFP-expressing neovasculature and activated endocardium at the injured area in cryoinjured hearts (Fig. 2A, lower row). These observations were supported by immunostaining of *tg(kdrl:mCherry)^{s896}* transgenic fish, in which mCherry expression is driven by the promoter for the endothelial VEGF receptor, *kdrl*. *Nrp1* immunostaining at 7 dpci in *tg(kdrl:mCherry)^{s896}* fish showed co-expression of mCherry-positive endocardium and *Nrp1* (Fig. S3). Furthermore, neovascularization was observed as early as 1 dpci in *tg(fli1a:EGFP)^{v1}* fish, consistent with previous findings (Marin-Juez et al., 2016), and these early neovessels also exhibited *Nrp1* expression (Fig. S4). *Nrp1* expression by tropomyosin-positive cardiomyocytes was low in control sham-operated hearts (Fig. 2B, upper row). However, following cryoinjury, *Nrp1* was expressed by a small population of cardiomyocytes located within the subepicardial layer at the lesion (Fig. 2B, lower row).

Epicardial expression of *Nrp1* was examined in *tg(wt1b:EGFP)^{li1}* zebrafish, in which EGFP expression is controlled by the promoter for the activated epicardial marker, *wt1b*. No detectable expression of EGFP was observed in sham-operated control hearts of *tg(wt1b:EGFP)^{li1}* zebrafish (Fig. 2C, upper row). By contrast, we observed high levels of colocalization between *Nrp1* and EGFP in the epicardium covering the lesion in cryoinjured *tg(wt1b:EGFP)^{li1}* zebrafish (Fig. 2C, lower row). Furthermore, immunofluorescent staining of *Wt1* and *Nrp1* in cryoinjured wild-type zebrafish revealed strong colocalization of *Wt1* with *Nrp1* in the epicardium adjacent to the injured area at 3 dpci (Fig. S5).

Nrp1a mutant zebrafish (*nrp1a^{sa1485}*) display delayed heart regeneration following cryoinjury

The marked upregulation of *nrp1* mRNA and protein at the borders of healthy and cryoinjured myocardium, and the expression of Nrps

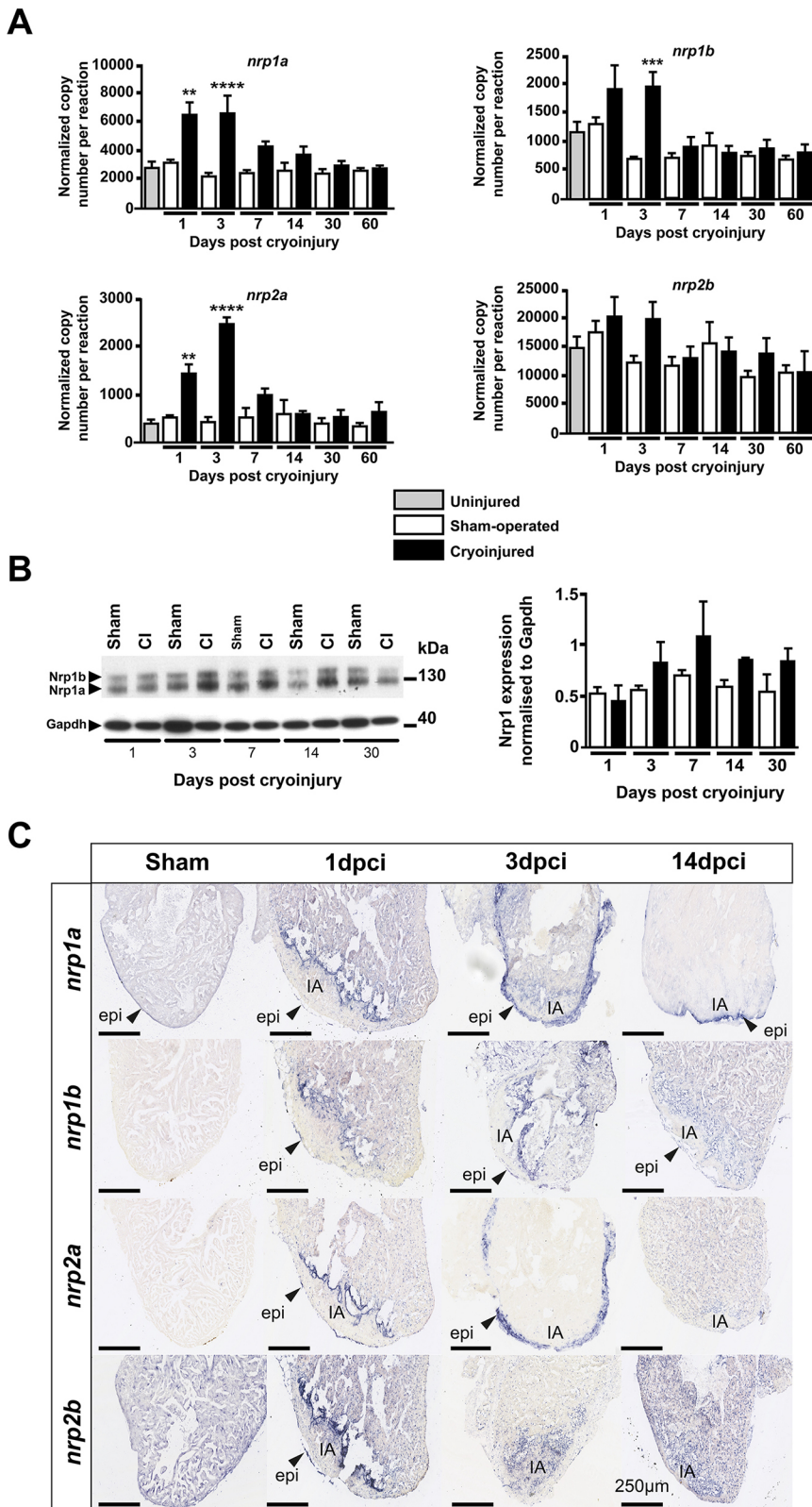


Fig. 1. Nrps are upregulated during zebrafish heart regeneration. (A) Absolute qPCR analysis of *nrp* family genes at 1, 3, 7, 14, 30 and 60 days following cryoinjury or sham surgery. Basal expression was evaluated in uninjured hearts of age-matched wild-type fish. Bars represent normalized copy number per reaction. Data are mean \pm s.e.m. ** P <0.01, *** P <0.005, **** P <0.001 (one-way ANOVA with Sidak's post hoc test for multiple comparisons of $n=4$ or 5 with each n being a pool of five ventricles). (B) Adult zebrafish ventricle lysates 1, 3, 7, 14 and 30 days following surgery, immunoblotted for Nrp1 and Gapdh (left); western blot quantification of Nrp1 protein in sham and cryoinjured ventricles 1, 3, 7, 14 and 30 days following surgery (right) ($n=4$ or 5, with each n being a pool of three ventricles). (C) *In situ* hybridization with digoxigenin-labeled antisense riboprobes were used to detect *nrp* family isoforms in sham-operated and cryoinjured adult zebrafish hearts 1, 3 and 14 dpci ($n\geq 3$). Arrowheads indicate gene expression within the epicardium. CI, cryoinjured; epi, epicardium; IA, injured area. Scale bars: 250 μ m.

by the endocardium and the activated epicardium suggested a role for Nrps in heart regeneration, particularly in the activated epicardium. Given the striking epicardial and endocardial expression of *nrp1a* after myocardial injury, we assessed the role of this isoform using the *nrp1a*^{sa1485} homozygous mutant zebrafish.

This mutant carries a nonsense mutation (tyrosine to ochre, TAA) at aa 206 (full length, 916 aa) in the second CUB domain of the *nrp1a* gene, resulting in the generation of a nonfunctional and truncated soluble N-terminal fragment (Fig. 3A). Given that the mutation occurs in the second CUB domain (also called a2), the binding of

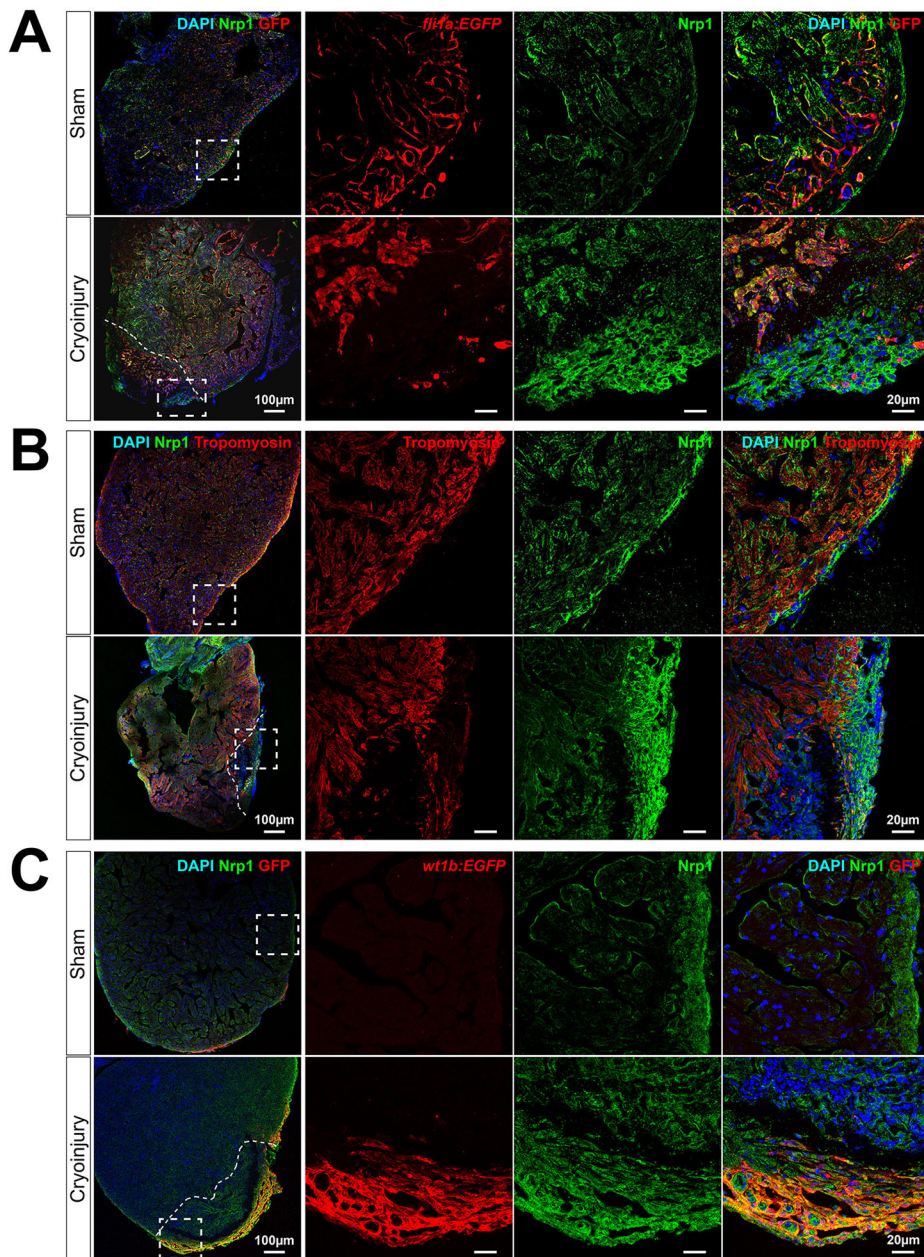


Fig. 2. Nrp1 is expressed by the endocardium and the epicardium in sham and cryoinjured hearts. (A–C) Immunostaining of 7 days post sham-operated (upper rows) and cryoinjured (lower rows) hearts. *Tg(fli1a:EGFP)^{Y1}* (A), wild-type fish immunostained for tropomyosin (B) and *tg(wt1b:EGFP)^{Y1}* (C) zebrafish hearts were used to identify endothelium, myocardium and activated epicardium, respectively ($n \geq 3$). The merged images are displayed with DAPI nuclei staining. Dashed boxes denote the location of enlarged images (right panels); dashed lines indicate the injury interface. Scale bars: 100 μm ; 20 μm in enlarged images.

both Vegf and Semaphorin 3A are predicted to be impaired in this mutant. The binding domain of other ligands, such as Fgf, Pdgf and Tgf, have not yet been fully characterized, but it is known the deletion probably prevents receptor oligodimerization or oligomerization and any resulting downstream signaling. Thus, the loss of *nrp1a* in these mutant fish has been shown to induce axons to misproject to the dorsal and anterior dorsal zone protoglomerulus (Taku et al., 2016). *Nrp1a^{sa1485}* mutant fish were viable, born at expected Mendelian ratios (Fig. 3B), displayed no obvious abnormal phenotype (Fig. S6A), and their body lengths and heart sizes were similar to those of wild-type fish (Fig. S6B–D). In the *nrp1a^{sa1485}* fish, *nrp1a* endogenous basal expression was significantly reduced at both the mRNA ($P < 0.0001$) (Fig. 3C,D) and protein ($P < 0.0001$) (Fig. 3E,F) levels, suggesting nonsense-mediated decay, whereas the other *nrp* family isoforms (*nrp1b*, *nrp2a* and *nrp2b*) were not significantly altered (*nrp1b*, $P = 0.71$; *nrp2a*, $P = 0.09$; and *nrp2b* $P = 0.06$) (Fig. 3C). Acid Fuchsin Orange

G (AFOG) staining was used to quantify the extent of the injury in both wild-type and *nrp1a^{sa1485}* fish over 60 days (Fig. 4A). Following cryoinjury, the extent of lesions in *nrp1a^{sa1485}* and wild-type fish hearts was similar, affecting $22.6 \pm 5.2\%$ (mean \pm s.e.m.) and $25.2 \pm 5.5\%$ of the ventricle, respectively (Fig. 4B). By 60 dpci, the injured area was almost cleared and new healthy myocardium had replaced the damaged tissue in wild-type fish (Fig. 4A,B). A reduction in the extent of heart repair was observed from as early as 7 dpci in *nrp1a^{sa1485}* hearts compared with wild-type hearts (Fig. 4A,B). Whereas fibrin deposits (red staining in injury area) were mostly cleared from the injury scars in wild-type fish by 14 dpci, fibrin deposits were still evident at 30 and 60 dpci in *nrp1a^{sa1485}* mutants (Fig. 4A). Quantification of the size of the cryoinjuries revealed an overall significant delay in the regeneration of mutant hearts compared with wild-type hearts (two-way ANOVA with Sidak's post hoc test for multiple comparisons, $P = 0.0208$) (Fig. 4B). Differences between *nrp1a^{sa1485}* and wild-type hearts

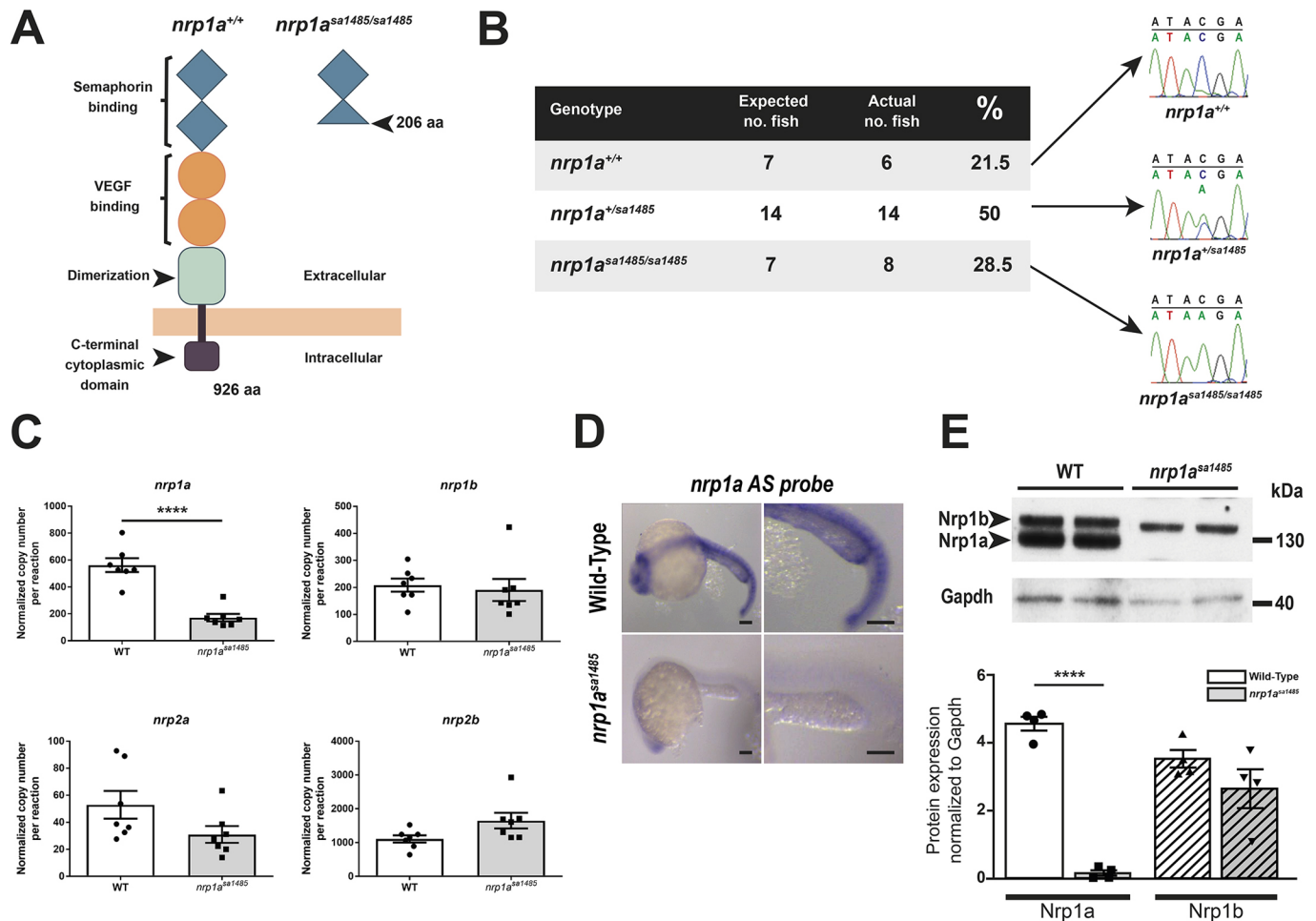


Fig. 3. Characterization of *nrp1a*^{sa1485} mutant fish. (A) Structure of Nrp1a in wild-type (*nrp1a*^{+/+}) (left) and *nrp1a*^{sa1485} mutant fish (right). The point mutation results in the generation of a premature stop codon at aa 206, resulting in a truncated Nrp1a fragment. Blue diamonds indicate CUB (a1 and a2) domains, orange circles indicate FA58C (b1 and b2) domains, the green square indicates the MAM domain and the brown square indicates the C-terminal domain. (B) Sequencing chromatograms of wild-type fish, heterozygous *nrp1a*^{sa1485/+} and homozygous *nrp1a*^{sa1485/sa1485} mutant fish. An early stop codon (nonsense mutation) TAA, replaces the wild-type TAC codon at aa 206. The genotypes of 14 zebrafish embryos 48 h post fertilization (hpf) were compared against the expected Mendelian ratio after heterozygous fish incross. (C) Absolute RT-qPCR of wild-type (WT; black circles, white bar) or *nrp1a*^{sa1485} homozygous mutant (black squares, gray bar) uninjured adult zebrafish hearts under basal conditions. *nrp1a* expression was significantly decreased in *nrp1a*^{sa1485} samples, suggesting nonsense-mediated decay. *****P*<0.0001 (two-tailed *t*-test; *n*=7 with each *n* being a pool of three ventricles). Data are means of normalized copy numbers per reaction ± s.e.m. (D) *Nrp1a* antisense (AS) *in situ* hybridization of wild-type (upper row) or *nrp1a*^{sa1485} homozygous mutant (lower row) embryos 24 hpf. *Nrp1a* expression was clearly decreased in *nrp1a*^{sa1485} samples. Scale bars: 50 μm. (E) Western blot of wild-type (WT) or *nrp1a*^{sa1485} homozygous mutant uninjured adult zebrafish ventricle lysates (top). Lysates were immunoblotted with an antibody targeting the Nrp1 cytoplasmic domain and Gapdh. Note the absence of C terminus detection of Nrp1a in the *nrp1a*^{sa1485} samples. Western blot quantification of Nrp1a (plain bars, circles for wild type, squares for *nrp1a*^{sa1485}) and Nrp1b (striated bars, upward triangles for wild type, downward triangles for *nrp1a*^{sa1485}) normalized to Gapdh (one-way ANOVA with Sidak's post hoc test for multiple comparisons of *n*=4), confirming the significant reduction in Nrp1a expression (*****P*<0.0001; plain white bar for wild type versus plain gray bar for *nrp1a*^{sa1485}), whereas Nrp1b was not significantly different between wild type (white striated bar) and *nrp1a*^{sa1485} (gray striated bar) (*P*=0.219) (bottom).

were also observed in the regeneration of the cortical layer and wound closure. In wild-type zebrafish hearts, regeneration typically led to formation of a continuous layer of cardiomyocytes enclosing the residual collagen scar, resulting in complete wound closure in the advanced stages of regeneration (30 and 60 dpci). By contrast, a larger proportion of mutant hearts at 30 and 60 dpci retained open wounds without complete closure of the lesion (Fig. 4C). We also quantified the surface area of the epicardium normalized to the length of the injury border to determine relative epicardial thickness in wild-type and *nrp1a*^{sa1485} mutants (Fig. 4D,E). We found a modest but significant reduction in epicardial thickness in mutant hearts at 3 dpci (*P*=0.048), suggesting a decrease in epicardial activation.

Revascularization of the cryoinjured heart tissue is impaired in *nrp1a*^{sa1485} mutant zebrafish

The impact of loss of functional Nrp1 on revascularization in cryoinjured hearts was examined by generating *nrp1a*^{sa1485} mutants in *tg(fli1a:EGFP)^{y1}* zebrafish, in which endothelial-specific Green Fluorescent Protein (GFP) expression is driven by the *fli1a* promoter. Angiogenesis occurs rapidly following heart injury in zebrafish, with a marked neovascular response evident as early as 1 dpci (Marín-Juez et al., 2016). Therefore, we compared the extent of angiogenesis in control *tg(fli1a:EGFP)^{y1}* and *nrp1a*^{sa1485} *tg(fli1a:EGFP)^{y1}* mutant zebrafish at 1 and 3 dpci. GFP-positive vessels were clearly identified within the injured area at 1 and 3 dpci in both wild-type and mutant zebrafish (Fig. 5A,B). However, the *nrp1a*^{sa1485} mutation was

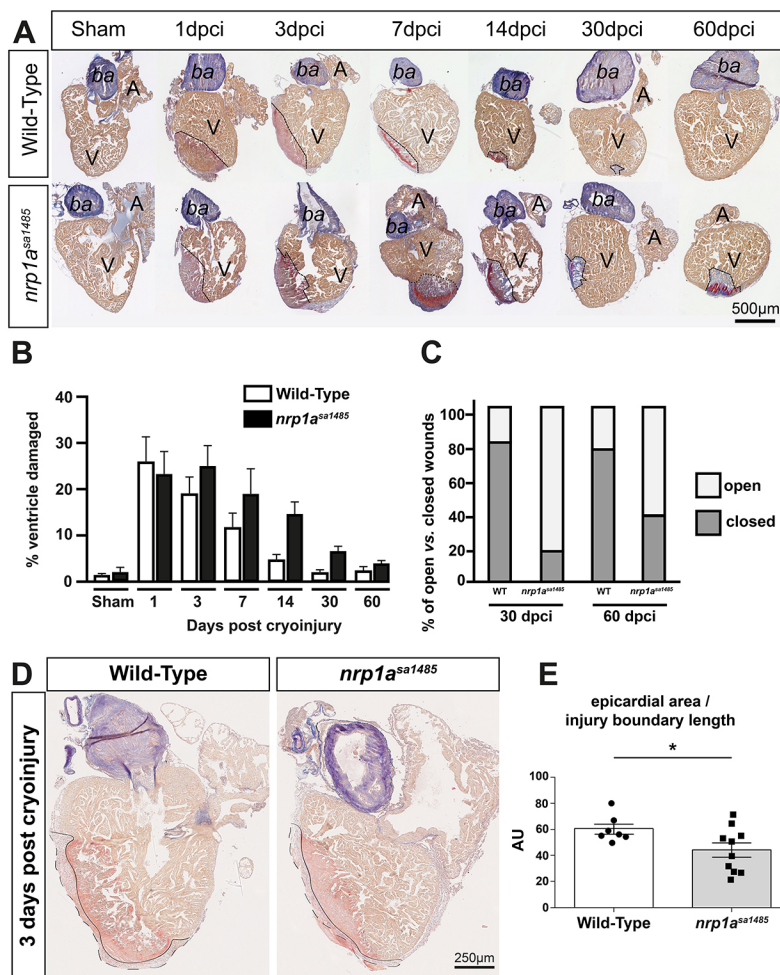


Fig. 4. Cardiac regeneration is delayed in *nrp1a^{sa1485}* mutants following cryoinjury.

(A) Heart sections from wild-type (top) and *nrp1a^{sa1485}* mutant (bottom) fish obtained at 1, 3, 7, 14, 30 and 60 dpci and stained with AFOG to identify the injured region. Dashed lines indicate the interface between cryoinjured and healthy tissue. (B) Cryoinjured areas were measured and represented as mean percentage of total ventricle area \pm s.e.m. $P < 0.05$ (two-way ANOVA with Sidak's post hoc test for multiple comparisons of $n = 4-8$). (C) A closed wound is one in which compact myocardium recovers following cryoinjury and encases the scar tissue; by contrast, a scar exposed to the surface is defined as an open wound. Wound closure was examined in wild-type (WT) and *nrp1a^{sa1485}* mutant hearts at 30 and 60 dpci and open versus closed wounds were expressed as a percentage of the total number of hearts ($n = 4-8$). (D, E) AFOG staining of wild-type and *nrp1a^{sa1485}* mutant hearts at 3 dpci (D) used to evaluate epicardial thickness and injury boundaries to calculate the epicardial area normalized to the length of the injury boundary (continuous line), quantified in E. Dashed line represents outer boundary of epicardial area. * $P < 0.05$ (two-tailed *t*-test of $n = 7$ for wild-type and $n = 10$ for *nrp1a^{sa1485}* hearts). A, atrium; ba, bulbus arteriosus; V, ventricle.

associated with a significant, 3- to 4-fold reduction in the extent of neovascularization. At 1 dpci, the average number of coronary vessels found within each microscopic field ($32,625 \mu\text{m}^2$) of the injury was 13 in wild-type zebrafish compared with three in *nrp1a^{sa1485}* mutant zebrafish ($P = 0.0087$) (Fig. 5C). At 3 dpci, the average number of newly formed vessels within the injured area per microscopic field of the injury was 19 in wild-type zebrafish compared with six in *nrp1a^{sa1485}* mutant zebrafish ($P = 0.0258$) (Fig. 5D).

We further examined angiogenesis in cryoinjured hearts from wild-type and *nrp1a^{sa1485}* mutant zebrafish at 3 dpci by immunofluorescent staining for the endothelial-specific marker TEK tyrosine kinase, endothelial (Tie2; also known as Tek, <https://zfinfo.org>). Use of Tie2 immunostaining as a reliable method to identify neovessels was verified by comparing the number of vessels within the cryoinjury of *tg(fli1a:EGFP)^{y1}* zebrafish identified either using Tie2 or GFP immunostaining (data not shown). Similar to the results discussed earlier, obtained with GFP staining of the *tg(fli1a:EGFP)^{y1}* transgenic line, the *nrp1a^{sa1485}* mutation was associated with a significant reduction in the extent of neovascularization as quantified by Tie2 staining of the neovessels (Fig. S7). At 3 dpci, the average number of coronary vessels found within each microscopic field of the injury was reduced by nearly 50% in *nrp1a^{sa1485}* mutants compared with wild-type zebrafish ($P = 0.0058$).

Epicardial activation is inhibited in *nrp1a^{sa1485}* hearts

We next addressed whether the delayed heart regeneration caused by loss of functional Nrp1 in *nrp1a^{sa1485}* zebrafish could be because

of an impact on activation of the epicardium and subsequent epicardial regeneration. Consistent with this possibility, our data showed epicardial upregulation of Nrp1 adjacent to the injured area, indicated by strong colocalization of Nrp1 with Wt1b, a specific marker for epicardial activation, at 3 dpci (Fig. 2C and Fig. S8A), a time coincident with robust epicardium activation during the reparative phase of the regeneration process (González-Rosa et al., 2017). To investigate this hypothesis further, we examined epicardial activation in cryoinjured hearts of wild-type and *nrp1a^{sa1485}* mutant *tg(wt1b:EGFP)^{li1}* zebrafish. Analysis of hearts at 3 dpci revealed a strong decrease in GFP expression under the control of the *wt1b* promoter in the *nrp1a^{sa1485}* mutants compared with wild type (Fig. 6A). Quantification of the percentage of GFP-positive cells within the epicardium covering the cryoinjured area confirmed a marked and significant reduction in the number of GFP-expressing activated epicardial cells in *nrp1a^{sa1485}* mutants (14.08% versus 26.4% for *nrp1a^{sa1485}* and wild type, respectively; $P = 0.0071$) (Fig. 6B). We also investigated whether loss of functional *nrp1a* impaired the proliferation of activated epicardial cells, using Proliferating Cell Nuclear Antigen (PCNA) staining (Fig. 6C). *Nrp1a^{sa1485}* hearts showed no statistically significant reduction in the proportion of proliferating epicardial cells expressing *wt1b* compared with wild-type hearts (37.25% versus 47.68% for *nrp1a^{sa1485}* and wild type, respectively; $P = 0.34$) (Fig. 6D). Given that WT1 is known to regulate epicardial EMT through the retinoic acid signaling pathway (von Gise et al., 2011), we investigated *aldh1a2* gene and protein expression in 3-dpci

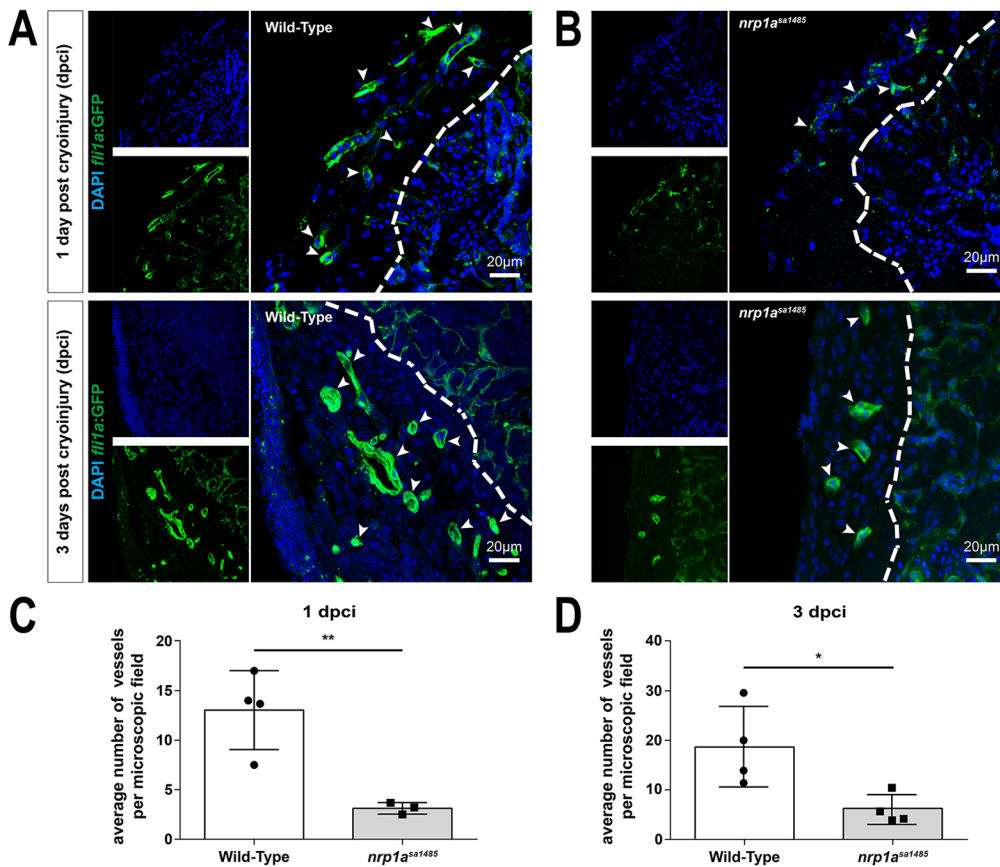


Fig. 5. Neovascularization of the cryoinjured area is impaired in *nrp1a^{sa1485}* mutants. (A,B) Blood vessels in either wild-type (A) or *nrp1a^{sa1485}* (B) *tg(fli1a:EGFP)^{y1}* zebrafish at 1 (upper row) and 3 (lower row) dpci were identified in heart sections using GFP immunofluorescence in vascular structures. Heart sections were also counterstained with DAPI. Smaller images (left) represent DAPI staining (blue) and GFP staining (vessels, green) only; larger images (right) are the merged images. The white dashed line delineates the border of the area of injury. White arrowheads indicate blood vessels. (C,D) GFP-positive vessels were quantified at 1 dpci (C; ** $P < 0.01$, two-tailed t -test of $n = 3$ and 4) and 3 dpci (D; * $P < 0.05$, two-tailed t -test of $n = 4$) for wild-type (white bars) versus *nrp1a^{sa1485}* (gray bars) hearts. Individual data points (circles for wild type and squares for *nrp1a^{sa1485}*) represent individual hearts, each averaged from vessel counts in three to four different sections covering the injury site.

hearts of wild-type and *nrp1a^{sa1485}* fish (Fig. 7). *aldh1a2* was upregulated following cryoinjury, but there was no significant difference between *aldh1a2* gene expression in wild-type and *nrp1a^{sa1485}* hearts ($P = 0.99$ for uninjured, $P = 0.97$ for 3 dpci) (Fig. 7C). We also stained Aldh1a2-positive cells in sections of 3-dpci heart (Fig. 7A) and quantified these cells in the endocardium, as well as the number of proliferating (PCNA-positive) Aldh1a2-positive cells (Fig. 7B). Our results revealed no significant difference in Aldh1a2-positive cells between wild-type and *nrp1a^{sa1485}* mutant hearts ($P = 0.43$ Aldh1a2⁺ cells, $P = 0.59$ PCNA+ Aldh1a2⁺ cells) (Fig. 7B).

The gene expression of other known EMT effectors, such as smooth muscle actin (*acta2*), *T-box 18* (*tbx18*), transforming growth factor beta receptor 1 a (*tgfb1a*), and Fgf receptor 2 and 4 (*fgfr2* and *fgfr4*), was unchanged in *nrp1a^{sa1485}* compared with wild-type hearts (data not shown). Thus, *nrp1b* might compensate for *nrp1a* inactivation in these pathways. In addition, the *nrp1a^{sa1485}* mutation did not result in an upregulation of the other neuropilin isoforms following cryoinjury (wild type versus *nrp1a^{sa1485}* for *nrp1b*, $P = 0.4674$; *nrp2a*, $P = 0.9026$; and *nrp2b*, $P = 0.051$) (Fig. S9).

Another known epicardial signaling effector downstream of WT1 is β -catenin (von Gise et al., 2011). To investigate the possibility that NRP1 is implicated in the regulation of β -catenin expression, we used the rat epicardial cell line described by Wada et al. (2003) and examined the effect in these cells of an adenovirus encoding a shRNA targeting NRP1 or a control adenovirus. We found that, after 48 h infection, there was a downregulation of β -catenin in NRP1-depleted cells compared with controls (Fig. 7D).

Additionally, we examined whether cardiomyocyte proliferation was affected in *nrp1a^{sa1485}* mutant hearts by determining the number of Myocyte Enhancer Factor 2C (Mef2C)-positive cells that

were also PCNA positive. We counted double positive cells both at the border and within the injured area and found that there was no significant difference in the number of proliferating cardiomyocytes ($P = 0.065$ and $P = 0.54$, respectively) (Fig. S10A,B).

Epicardial expansion and activation of cryoinjury-induced *nrp1a^{sa1485}* heart explants is impaired

We next examined the role of Nrp1 in epicardial activation in an *ex vivo* heart explant model (Kim et al., 2012). Immunofluorescent staining of Nrp1 in explants of wild-type ventricular apexes collected at 5 dpci and cultured *in vitro* for 7 days showed perinuclear, cytoplasmic and membrane localization (Fig. S8B). Epicardial culture from *tg(wt1b:EGFP)^{li1}* ventricles showed that *Wt1b:EGFP* expression was variable in these explants and was strongly expressed by a subpopulation of explanted epicardial cells (Fig. 8C, top row).

wt1b:EGFP expression was increased in explant outgrowths from cryoinjured compared with those from control, sham-operated hearts (Fig. S11A,C) and, similar to resected hearts (Kim et al., 2012), explants from wild-type cryoinjured hearts generated greater outgrowth compared with those from wild-type sham-operated hearts ($P = 0.0001$; Fig. 8A,B). We next assessed the role of Nrp1a in injury-induced epicardial activation using epicardial explants from wild-type and *nrp1a^{sa1485}* *tg(wt1b:EGFP)^{li1}* zebrafish. Epicardial outgrowths of cryoinjury-induced *nrp1a^{sa1485}* heart explants were markedly impaired compared with wild-type explants ($P = 0.0009$) (Fig. 8A,B) and we observed no significant difference between the outgrowths of either wild-type or *nrp1a^{sa1485}* mutant sham-operated hearts ($P = 0.93$ and $P = 0.99$, respectively). Furthermore, *nrp1a^{sa1485}* explants showed a marked decrease in GFP expression compared with wild-type hearts, both at the edge of the explant and within the

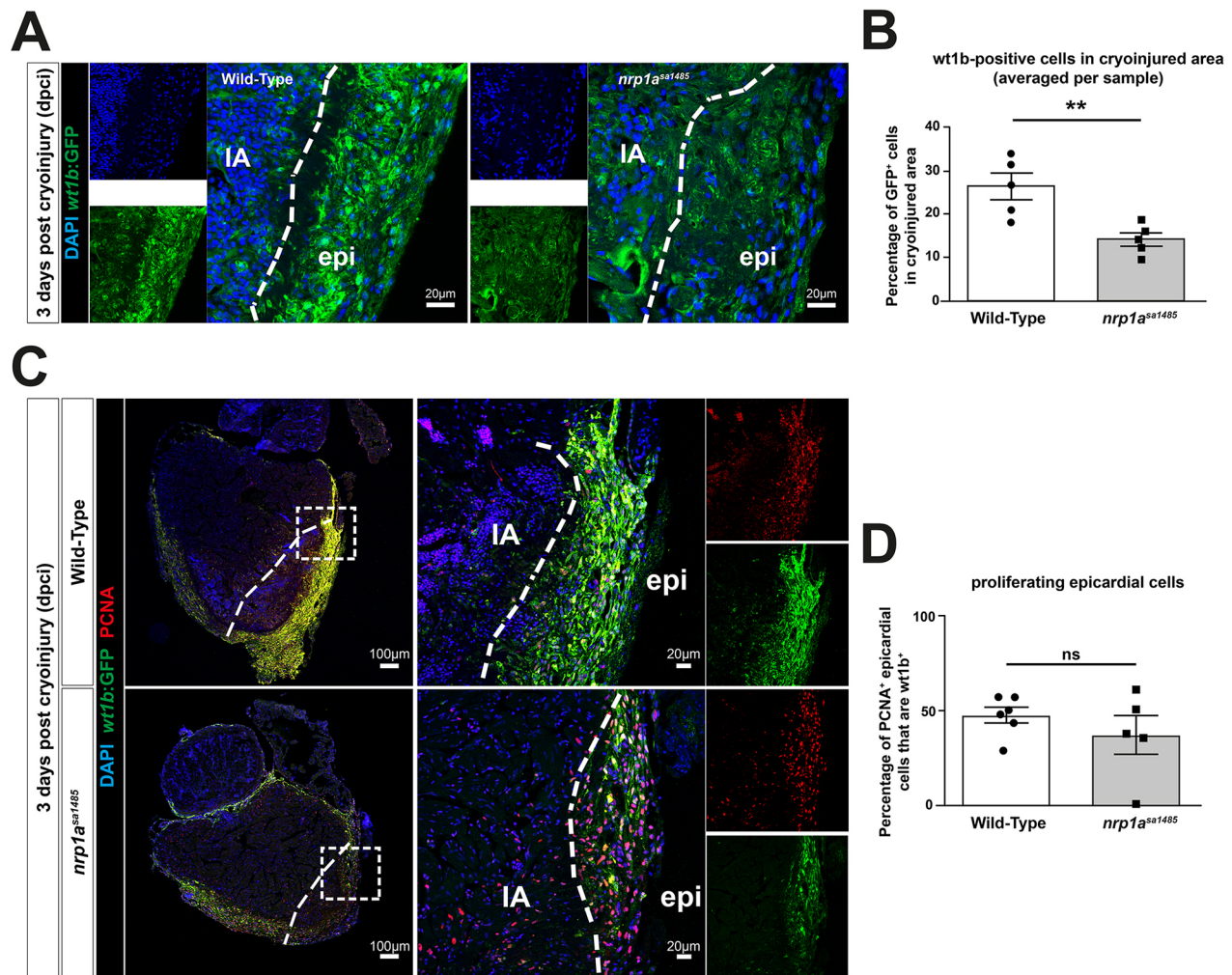


Fig. 6. Epicardial activation is decreased in *nrp1a^{sa1485}* hearts following cryoinjury. (A–D) Wild-type and *nrp1a^{sa1485}* mutant cryoinjured fish on the *tg(wt1b:EGFP)^{li1}* background were analyzed for epicardial activation at 3 dpci by identification of *wt1b:EGFP*-positive cells (A,C), and were also stained with DAPI (blue; A,C) and anti-PCNA antibodies (red; C), as indicated. In A, smaller images represent DAPI staining (blue) and GFP staining (activated epicardium, green) only; larger images are the merged images. In C, boxed area in left panel is enlarged in the middle. Smaller images (right) represent PCNA staining (red) and GFP staining (activated epicardium, green) only; larger images in the middle are the merged images. (B) Quantification of percentages of *wt1b:EGFP*-positive cells adjacent to the area of cryoinjury (indicated by the dashed line in A,C) in wild-type (white bar) and *nrp1a^{sa1485}* (gray bar) mutant fish. $**P < 0.01$ (two-tailed *t*-test of $n=5$). (D) Quantification of percentages of cells positive for *wt1b:EGFP* and PCNA in the area of cryoinjury. $P > 0.05$ [two-tailed *t*-test of $n=6$ and 5 for wild-type (white bar) and *nrp1a^{sa1485}* (gray bar), respectively]. Individual data points (circles for wild type and squares for *nrp1a^{sa1485}*) represent percentages in individual hearts, each averaged from counts in two to four different sections covering the injury borders. epi, epicardium; IA, injury area; ns, not significant. White-dotted line delineates injury–epicardial border.

region closest to the heart (Fig. 8C), providing further support for a loss of epicardial activation in the *nrp1a^{sa1485}* mutants compared with wild-type hearts. This confirmed our observations of reduced GFP-positive epicardial cells in sections from cryoinjured *nrp1a^{sa1485} tg(wt1b:EGFP)^{li1}* zebrafish hearts (Fig. 6A,B). The less marked effect of the *nrp1a^{sa1485}* mutant on epicardial activation observed in heart sections compared with cultured epicardial explants, might reflect compensatory effects of other cell types (such as fibroblasts or immune cells) secreting paracrine factors to drive epicardial activation and partially rescue the *nrp1a* mutant phenotype *in vivo*, which are lacking in epicardial cultures. Cao et al. (2017) recently showed that transient hypertrophy and polyploidization have an important role in epicardial regeneration following induced cell death in the zebrafish heart. To investigate whether changes in cell size or ploidy had a role in the effect of the *nrp1a^{sa1485}* mutant on injury-induced epicardial regeneration, we also analyzed the size and ploidy of the cells at the center and at the

edge of the ventricular explant (Fig. 8D). There was no significant difference in cell size, neither at the center ($P=0.53$) nor at the edge of the explant ($P=0.57$), but we observed a reduction in the number of polyploid cells at the edge of the explant in the *nrp1a^{sa1485}* mutants compared with wild-type hearts ($P=0.016$), whereas there was no difference in the center of the explant ($P=0.46$).

DISCUSSION

Epicardial activation and angiogenesis are processes essential for zebrafish heart regeneration following injury. During these processes, revascularization and injury-induced EMT are driven by Vegf, Fgf and Pdgf (Chablais and Jazwinska, 2012; Kim et al., 2010; Lepilina et al., 2006), which are all ligands for the cell surface receptor Nrp1. Although it is known that NRPs are essential for angiogenesis and are increasingly implicated in EMT in other contexts in mammals (Adham et al., 2014; Chu et al., 2014; Kawasaki et al., 1999), their role has not previously been

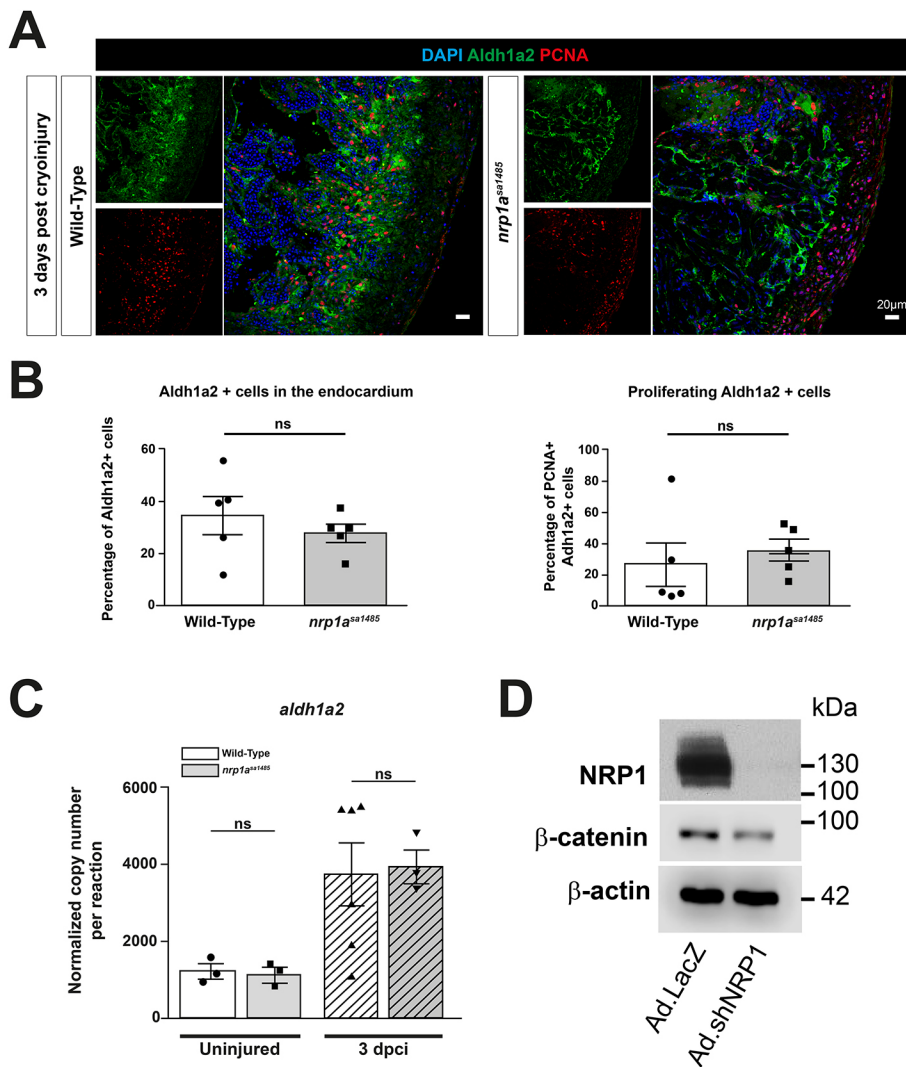


Fig. 7. Aldh1a2 expression is unchanged in *nrp1a^{sa1485}* fish following cryoinjury.

(A-D) β-Catenin expression is downregulated in rat epicardial cells. (A) Cryoinjured wild-type and *nrp1a^{sa1485}* fish were analyzed for Aldh1a2 expression and were also stained with DAPI and anti-PCNA antibody at 3 dpci. (B) Percentage of Aldh1a2-positive cells in the endocardium of the cryoinjury area (left) and percentage of proliferating endocardial cells (PCNA⁺ and Aldh1a2⁺ cells) (right). $P=0.43$ for Aldh1a2⁺ cells and $P=0.59$ for PCNA⁺ Aldh1a2⁺ cells (two-tailed *t*-test of $n=5$). (C) Absolute qPCR analysis of *aldh1a2* expression was performed on uninjured and 3 dpci ventricles from wild-type and *nrp1a^{sa1485}* mutant fish. Bars represent normalized copy number per reaction mean \pm s.e.m. (one-way ANOVA with Sidak's post hoc test for multiple comparisons of $n \geq 3$). (D) Rat epicardial cells were cultured *in vitro* and infected with control (Ad.LacZ) and shRNA NRP1 (Ad.shNRP1) adenoviral constructs. Cell lysates immunoblotted for NRP1, β-catenin and β-actin ($n=2$). ns, not significant. Scale bars: 20 μm.

characterized in zebrafish heart regeneration. Here, we show for the first time that *nrp1* and *nrp2* are upregulated in response to cardiac injury and that *nrp1a* has a role in revascularization and epicardial activation and migration, processes that are essential for the regeneration of the zebrafish heart.

Nrp1a, *nrp1b*, *nrp2a* and *nrp2b* mRNAs were all strongly upregulated in the zebrafish heart 1-3 days after cryoinjury, coinciding with the time of epicardial activation, which occurs very early following cardiac injury (Cao and Cao, 2018). Increased protein expression of both Nrp1 isoforms also occurred 3-14 days following cryoinjury, further supporting the conclusion that Nrp1 is upregulated in the early regenerating heart. Our results also revealed a striking spatiotemporal upregulation of the *nrp* family isoforms. Specifically, *nrp2a* was strongly upregulated in the endocardium (1 dpci) and in the epicardium proximal to the injury (3 dpci), whereas *nrp1a* was strongly upregulated in the same regions at 1, 3 and 14 dpci. These findings support a sustained role for these isoforms in heart regeneration, particularly in the epicardial activation phase, which occurs during the first 3-7 days of regeneration. Although the lack of suitable reagents made further detailed studies of Nrp2 problematic, a role for Nrp1 in epicardial activation in response to heart injury was further supported by immunofluorescent staining demonstrating colocalization of Nrp1 with both endogenous Wt1 and with EGFP under the control of the

wt1b promoter. This is an embryonic gene that is upregulated following cardiac injury and is an activated epicardium marker (Peralta et al., 2014; von Gise et al., 2011).

Analysis of mutant *nrp1a^{sa1485}* fish lacking expression of full-length Nrp1a provided direct evidence that Nrp1a is required for zebrafish heart regeneration. *Nrp1a^{sa1485}* fish displayed no morphological or pathological phenotype. It was previously reported that knockdown of *nrp1* using morpholino oligomers produces a lethal phenotype in zebrafish embryos (Martyn and Schulte-Merker, 2004). The absence of embryonic lethality in *nrp1a^{sa1485}* fish compared with *nrp1a* morpholino knockdown probably reflects redundancy because of adaptive mechanisms relying on compensation by *nrp1b* and also suggest morpholino off-target effects in *nrp1a* morphants (Kok et al., 2015). The genetic robustness of the *nrp1a^{sa1485}* mutant fish could also be the result of the allele displaying mutant mRNA decay (El-Brolosy et al., 2019), although we could not detect any compensative upregulation of the other *nrp*-related genes. Following cardiac damage, *nrp1a^{sa1485}* mutants exhibited a significantly reduced regenerative response compared with wild-type controls. The importance of *nrp1a* for heart regeneration was demonstrated by the delayed and incomplete removal of fibrin deposits essential for the scar resolution process in *nrp1a^{sa1485}* mutant fish. Given that myocardial proliferation was not significantly affected in *nrp1a^{sa1485}* mutant fish, delayed wound

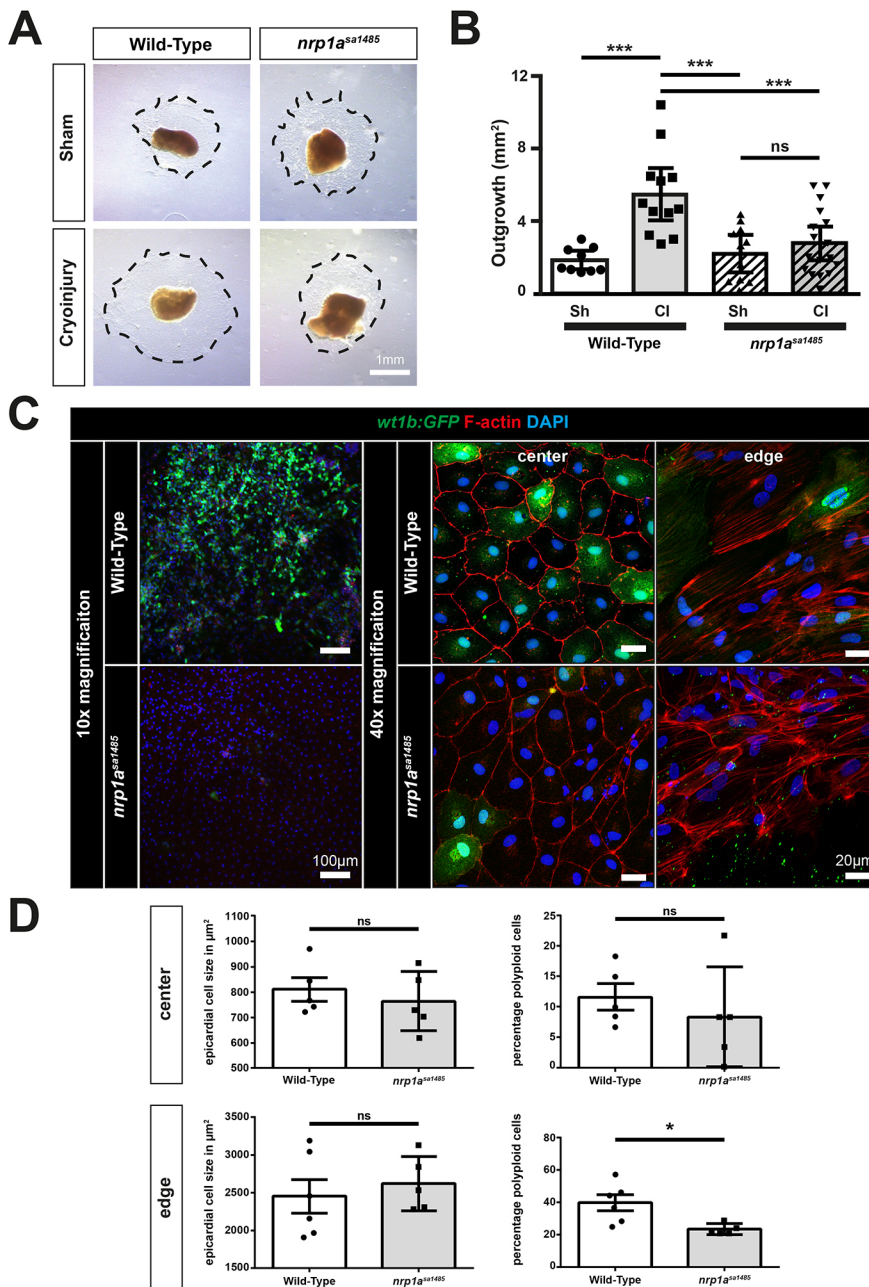


Fig. 8. Epicardial cryoinjury-induced expansion and activation are impaired in *nrp1a*^{sa1485} mutants.

(A–D) The apices of wild-type and *nrp1a*^{sa1485} zebrafish ventricles were collected 5 days post sham surgery or cryoinjury and cultured on fibrin gels for 7 days. (A) Epicardial cells migrated into the fibrin gels (dotted black lines). (B) Epicardial outgrowths were measured for each condition (sh, sham-operated and CI, cryoinjured hearts) after 7 days culture. Data are mean outgrowth area (mm²) ± s.e.m. ****P* < 0.001 (one-way ANOVA with Sidak's post hoc test for multiple comparisons of *n* > 9). (C) Epicardial explant recovered from wild-type and *nrp1a*^{sa1485} *tg(wt1b:EGFP)*^{fl1} cryoinjured fish at 5 dpca were left to grow on fibrin gels for 7 days and stained for GFP. GFP fluorescence was observed at 10× (left column) and 40× magnification at the center and the periphery of the explants (middle and right columns, respectively). (D) Cell size (left) and ploidy (right) were quantified both at the center (top row) and at the edge (bottom row) of the explant. Data are expressed as percentage of cells per field of view ± s.e.m. Each *n* represents an average of 3 fields of view per explant (two-tailed *t*-test of *n* ≥ 5); **P* < 0.05. ns, not significant. Scale bars: 1 mm in A, 20 μm in C (right); 100 μm in C (left).

closure in *nrp1a*^{sa1485} fish probably indicates a failure of the myocardium to migrate efficiently towards the subepicardial layer after cryoinjury. Together, these findings provide strong evidence that *nrp1a* is required for zebrafish heart regeneration following cryoinjury. Given that we examined the loss of only the *nrp1a* isoform, because of the anticipated embryonic lethality of a double *nrp1a* and *nrp1b* knockout, it is possible that Nrp1 loss would have an even more prominent role in heart regeneration in species that did not undergo genome duplication. Furthermore, our data also showed epicardial expression of *nrp2a* and *nrp2b*, indicating a possible role of Nrp2 isoforms in epicardial activation and heart regeneration, something that warrants further investigation.

Activation of the epicardium and subsequent regeneration involves multiple cellular processes, including cell migration, proliferation and EMT. It is well established that NRP1 modulates cell migration in diverse mammalian cell types (Evans et al., 2011;

Pellet-Many et al., 2008; Wang et al., 2003). The conclusion that *nrp1a* is important for zebrafish epicardial migration is supported by our finding that *ex vivo* outgrowth from epicardial explants of *nrp1a*^{sa1485} hearts was also impaired. Furthermore, we observed a reduction in polyploidization of explanted epicardial cells in *nrp1a*^{sa1485} hearts, a process that was recently implicated as an important mechanism underlying epicardial regeneration following induced cell death in zebrafish (Cao et al., 2017). By contrast, we observed no effect on epicardial cell proliferation in cryoinjured *nrp1a*^{sa1485} hearts, indicating that *nrp1a* is not crucial for proliferation, in line with studies of NRP1 function in primary mammalian cells. However, we cannot preclude the possibility that one of the other Nrp isoforms has a role in epicardial proliferation.

Reduced *in vitro* expansion of *nrp1a*-deficient epicardial cells could have been the result of impaired detection of cellular cues promoting migration. Consistent with this possibility, we observed

upregulation of Nrp1 isoform expression concomitant with increased expression of *tgfb*, *pdgfab*, *vegfc* and the receptor *pdgfrb*, chemotactic factors and receptors implicated in zebrafish heart regeneration, and also shown to act as ligands and co-receptors for NRP1 in mediating mammalian cellular functions. Interestingly, using the (*wt1b:EGFP*)^{fl} transgenic fish line, we also noted that the *nrp1a*^{sa1485} epicardial cells failed to re-express the *wt1b* embryonic marker *in vitro* as well as *in vivo*. Previously, González-Rosa et al. (2012) demonstrated the importance of *wt1b:EGFP*⁺ epicardial derived cells (EPDCs) in the regeneration process that gives rise to perivascular fibroblasts and myofibroblasts and that these cells also participated in the regeneration process by secreting essential proangiogenic paracrine factors. Therefore, the decreased number of GFP-expressing (and, therefore, *wt1b*⁺) EPDCs in the *nrp1a*^{sa1485} hearts probably explains their delayed regeneration compared with wild-type hearts. WT1 regulates epicardial EMT through β -catenin and retinoic acid signaling pathways in mice (von Gise et al., 2011) and interruption of Wnt/ β -catenin signaling in epicardial cells disrupts EMT and compromises cardiac function after acute cardiac injury (Duan et al., 2012). Although we observed an upregulation of *aldh1a2* gene and protein expression in cryoinjured hearts in both *nrp1a*^{sa1485} wild-type fish, there was no significant difference in either gene or protein expression at 3 dpci, indicating that Nrp1 functions in epicardial regeneration via *Aldh1a2*-independent pathways downstream of *Wt1b*.

Our study also revealed Nrp1 upregulation following cardiac damage by the activated endocardium, which undergoes endothelial to mesenchymal transition (endoMT) in response to injury (Kikuchi et al., 2011), by the neovasculature and by some subepicardial cardiomyocytes known to be a primary source of new myocardium (Kikuchi et al., 2010). Following injury, these cells acquire a migratory phenotype to contribute to the regenerative processes in the heart. It is probable that the *nrp1a*^{sa1485} endocardium is less able to perform this function, further contributing to the overall observed delay in regeneration.

Nrp1 has an essential role in angiogenesis in mammalian and zebrafish development, and is required in postnatal and adult angiogenic processes (Lee et al., 2002; Soker et al., 1998). Marín-Juez et al. recently reported transient upregulation of *vegfaa* at 1 dpci, with a return to baseline expression by 3 dpci, and showed an important role for *vegfaa* in inducing rapid early revascularization of the injured heart (Marín-Juez et al., 2016). Based on RT-qPCR, our data showed a trend towards increased *vegfaa* expression at 1 dpci, although this was not statistically significant, unlike the concomitant changes in *nrp1*. Similarly to its major endothelial ligand *vegfaa*, the main Nrp1 co-receptor *kdr1* was also not significantly upregulated. However, we observed revascularization of the injured area as early as 1 dpci, in line with previous findings (Marín-Juez et al., 2016). These neovessels also expressed Nrp1, and studies in *nrp1a*^{sa1485} mutants co-expressing *flila:EGFP*^{v1} demonstrated a role for *nrp1a* in the revascularization of the cryoinjured area. As expected, the loss of Nrp1a reduced the number of neovessels in the regenerating heart of *nrp1a*^{sa1485} fish compared with their wild-type counterparts. Although our findings are consistent with a role for Nrp1 in mediating *Vegfaa*-driven angiogenesis in the regenerating heart, recent findings indicate that the role of NRP1 in developmental angiogenesis might be largely independent of VEGF, because NRP1 mutations that prevent VEGFA binding impair postnatal angiogenesis but are compatible with normal embryonic development (Fantin et al., 2015; Fantin et al., 2014). Therefore, it is plausible that the angiogenic role of Nrp1 in revascularization of

the regenerating zebrafish heart is also mediated via binding of other ligands to Nrp1 (Ball et al., 2010; Pellet-Many et al., 2011; West et al., 2005).

This study establishes a novel role for Nrp1 in epicardial activation and angiogenesis during zebrafish heart regeneration following injury. Further work to elucidate the extracellular ligands for Nrp1 in epicardial and endothelial cells and the signaling pathways that mediate its role further downstream will shed new light on the mechanisms involved in epicardial activation in heart regeneration.

MATERIALS AND METHODS

Zebrafish husbandry and cryoinjury

Procedures were performed in accordance with the Animals (Scientific Procedures) Act 1986, and husbandry was regulated by the central University College London fish facility. Cryoinjury procedure was carried out as described by González-Rosa and Mercader (2012), and more details are provided in the supplementary Materials and Methods.

RT-qPCR

Ventricles from corresponding time-points and treatments were pooled for RNA extraction using the RNeasy Mini Kit (Qiagen). RNA was reverse transcribed using the QuantiTect[®] Reverse Transcription Kit (Qiagen). All primers (details are described in Table S1) and standards were purchased from qStandard[®] and absolute qPCR was performed by qStandard[®]. More details are provided in the supplementary Materials and Methods.

Histological procedures

In situ hybridization, immunofluorescence and AFOG procedures are described in the supplementary Materials and Methods.

Fibrin gel heart explants

In vitro epicardial cell outgrowth experiments were performed as previously described (Kim et al., 2012). The apices of cryoinjured and sham-operated zebrafish hearts were isolated 5 days post surgery and placed firmly on set fibrin gel matrices, ensuring epicardial surface contact with the gel. Medium was changed every 2 days and cells were cultured for 7 days before harvesting epicardial outgrowths for protein extraction or immunofluorescence imaging. More details are provided in the supplementary Materials and Methods.

Immunoblotting

Epicardial cell lysates were obtained from a single well of a six-well plate and zebrafish heart lysates from a minimum of three ventricles pooled together. Protein contents were separated using SDS-PAGE, electro-transferred to PVDF membranes and blocked in 5% milk in PBS containing 0.1% Tween-20 (PBST). Membranes were incubated with primary antibodies overnight at 4°C. Western blot band densities were normalised to GAPDH and analysed using ImageJ. Blots were washed with PBST and proteins detected using HRP-conjugated secondary antibodies and ECL detection with Hyperfilm. More details about protein extraction, antibodies and immunoblotting protocol are provided in the supplementary Materials and Methods.

Recombinant adenovirus generation

Rat-specific NRP1 shRNA construct was generated as previously described (Pellet-Many et al., 2015), and adenovirus generation and reagents are detailed in the supplementary Materials and Methods.

Epicardial cell NRP1 knockdown

Rat epicardial cells were a generous gift from Dr Nicola Smart (Department of Physiology, Anatomy and Genetics, University of Oxford, UK) and are described in Wada et al. (2003). Cells were infected with adenovirus at a multiple of infection (MOI) of 100 for 24 hours before protein extraction and subsequent immunoblotting as described above. See supplementary Materials and Methods for more details.

Statistical analysis

All results are presented as mean±s.e.m. Experimental repeat *n* values are indicated as individual data points in graphs or are specified in figure legends. When samples were pooled to produce 1 *n* (e.g. for qPCR) or several sections per tissue were analyzed, this is indicated in the figure legends or the main text. All data were visualized and analyzed using Graphpad prism 6.0 software. All data were first tested for normal distribution using histograms and the D'Agostino–Pearson Omnibus test. Comparisons of more than two groups (e.g. AFOG cryoinjury area and qPCR data) were analyzed for statistical significance using one-way ANOVA with preselected pairs and the Sidak's post hoc test for multiple comparisons and, for overall effect, a two-way ANOVA with Tukey post-test was conducted. Student's unpaired *t*-tests were applied to all other data sets, (i.e. for data sets comparing only two groups). The Mann–Whitney test was applied for comparisons of two groups if data were not normally distributed. Statistical significance values are indicated in figure legends and in the main text. Data were considered significant at *P*<0.05. All immunostaining data were analyzed by a blinded investigator.

Acknowledgements

We thank Juan Manuel González Rosa for teaching us the cryoinjury model, Dr Gaia Gestri for her help with the ISH protocol and for providing us with the *tg(kdrl:mCherry)*⁸⁹⁶ fish, Dr Shanie Budhram-Mahadeo for her advice to generate the ISH probes and Dr Stefan Schulte-Merker for the pCR11 vector used for generating the *nrp2b* ISH probe. We also acknowledge Roisin Brid Doohan and Dr Mathilda Mommersteeg for advising on histological procedures, Dr Patricia De Winter and Dr David Sugden (qStandard[®]) for qPCR services, and the University College London central fish facility for *in vitro* fertilization of *nrp1a*^{sa1485} fish line and maintenance of fish stocks.

Competing interests

The authors declare no competing or financial interests.

Author contributions

Conceptualization: V.L., I.C.Z., C.P.-M.; Methodology: V.L., L.W., N.M.-H., C.P.-M.; Validation: V.L., L.W.; Formal analysis: V.L., L.W., J.S., I.C.Z., C.P.-M.; Investigation: V.L., L.W., J.S., I.E., C.P.-M.; Resources: N.M.-H.; Writing – original draft: V.L., I.C.Z., C.P.-M.; Writing – review & editing: V.L., L.W., P.F., I.C.Z., C.P.-M.; Supervision: P.F., I.C.Z., C.P.-M.; Project administration: I.C.Z., C.P.-M.; Funding acquisition: I.C.Z., C.P.-M.

Funding

This work was supported by the following grants: British Heart Foundation doctoral training grants (FS12/70/30009 to V.L. and FS16/41/32235 to L.W.), British Heart Foundation project grant PG16/84/32464 (to C.P.-M. and I.C.Z.), British Heart Foundation project grant PG17/87/33400 (to I.E. and I.C.Z.) and British Heart Foundation programme grant RG/06/003 (to I.C.Z.). Deposited in PMC for immediate release.

Supplementary information

Supplementary information available online at <http://dev.biologists.org/lookup/doi/10.1242/dev.174482.supplemental>

References

- Adham, S. A. I., Al Harrasi, I., Al Haddabi, I., Al Rashdi, A., Al Sinawi, S., Al Maniri, A., Ba-Omar, T. and Coomber, B. L. (2014). Immunohistological insight into the correlation between neuropilin-1 and epithelial-mesenchymal transition markers in epithelial ovarian cancer. *J. Histochem. Cytochem.* **62**, 619–631. doi:10.1369/0022155414538821
- Ball, S. G., Bayley, C., Shuttleworth, C. A. and Kielty, C. M. (2010). Neuropilin-1 regulates platelet-derived growth factor receptor signalling in mesenchymal stem cells. *Biochem. J.* **427**, 29–40. doi:10.1042/BJ20091512
- Cahill, T. J. and Kharbanda, R. K. (2017). Heart failure after myocardial infarction in the era of primary percutaneous coronary intervention: mechanisms, incidence and identification of patients at risk. *World J. Cardiol.* **9**, 407–415. doi:10.4330/wjcv.9.v9.i5.407
- Cao, Y. and Cao, J. (2018). Covering and re-covering the heart: development and regeneration of the epicardium. *J. Cardiovasc. Dev. Dis.* **6**, 3. doi:10.3390/jcd6010003
- Cao, J. and Poss, K. D. (2018). The epicardium as a hub for heart regeneration. *Nat. Rev. Cardiol.* **15**, 631–647. doi:10.1038/s41569-018-0046-4
- Cao, J., Wang, J., Jackman, C. P., Cox, A. H., Trembley, M. A., Balowski, J. J., Cox, B. D., De Simone, A., Dickson, A. L., Di Talia, S. et al. (2017). Tension

- creates an endoreplication wavefront that leads regeneration of epicardial tissue. *Dev. Cell* **42**, 600–615.e4. doi:10.1016/j.devcel.2017.08.024
- Chablais, F. and Jazwinska, A. (2012). The regenerative capacity of the zebrafish heart is dependent on TGFbeta signaling. *Development* **139**, 1921–1930. doi:10.1242/dev.078543
- Chablais, F., Veit, J., Rainer, G. and Jaźwińska, A. (2011). The zebrafish heart regenerates after cryoinjury-induced myocardial infarction. *BMC Dev. Biol.* **11**, 21. doi:10.1186/1471-213X-11-21
- Chu, W., Song, X., Yang, X., Ma, L., Zhu, J., He, M., Wang, Z. and Wu, Y. (2014). Neuropilin-1 promotes epithelial-to-mesenchymal transition by stimulating nuclear factor-kappa B and is associated with poor prognosis in human oral squamous cell carcinoma. *PLoS ONE* **9**, e101931. doi:10.1371/journal.pone.0101931
- Dobaczewski, M., Gonzalez-Quesada, C. and Frangogiannis, N. G. (2010). The extracellular matrix as a modulator of the inflammatory and reparative response following myocardial infarction. *J. Mol. Cell. Cardiol.* **48**, 504–511. doi:10.1016/j.yjmcc.2009.07.015
- Duan, J., Gherghe, C., Liu, D., Hamlett, E., Srikantha, L., Rodgers, L., Regan, J. N., Rojas, M., Willis, M., Leask, A. et al. (2012). Wnt1/betacatenin injury response activates the epicardium and cardiac fibroblasts to promote cardiac repair. *EMBO J.* **31**, 429–442. doi:10.1038/emboj.2011.418
- El-Brolosy, M. A., Kontarakis, Z., Rossi, A., Kuenne, C., Gunther, S., Fukuda, N., Kikhi, K., Boezio, G. L. M., Takacs, C. M., Lai, S. L. et al. (2019). Genetic compensation triggered by mutant mRNA degradation. *Nature* **568**, 193–197. doi:10.1038/s41586-019-1064-z
- Evans, I. M., Yamaji, M., Britton, G., Pellet-Many, C., Lockie, C., Zachary, I. C. and Frankel, P. (2011). Neuropilin-1 signaling through p130Cas tyrosine phosphorylation is essential for growth factor-dependent migration of glioma and endothelial cells. *Mol. Cell. Biol.* **31**, 1174–1185. doi:10.1128/MCB.00903-10
- Fantin, A., Herzog, B., Mahmoud, M., Yamaji, M., Plein, A., Denti, L., Ruhrberg, C. and Zachary, I. (2014). Neuropilin 1 (NRP1) hypomorphism combined with defective VEGF-A binding reveals novel roles for NRP1 in developmental and pathological angiogenesis. *Development* **141**, 556–562. doi:10.1242/dev.103028
- Fantin, A., Lampropoulou, A., Gestri, G., Raimondi, C., Senatore, V., Zachary, I. and Ruhrberg, C. (2015). NRP1 regulates CDC42 activation to promote filopodia formation in endothelial tip cells. *Cell Rep.* **11**, 1577–1590. doi:10.1016/j.celrep.2015.05.018
- Glinka, Y. and Prud'homme, G. J. (2008). Neuropilin-1 is a receptor for transforming growth factor beta-1, activates its latent form, and promotes regulatory T cell activity. *J. Leukoc. Biol.* **84**, 302–310. doi:10.1189/jlb.0208090
- González-Rosa, J. M. and Mercader, N. (2012). Cryoinjury as a myocardial infarction model for the study of cardiac regeneration in the zebrafish. *Nat. Protoc.* **7**, 782–788. doi:10.1038/nprot.2012.025
- González-Rosa, J. M., Martín, V., Peralta, M., Torres, M. and Mercader, N. (2011). Extensive scar formation and regression during heart regeneration after cryoinjury in zebrafish. *Development* **138**, 1663–1674. doi:10.1242/dev.060897
- González-Rosa, J. M., Peralta, M. and Mercader, N. (2012). Pan-epicardial lineage tracing reveals that epicardium derived cells give rise to myofibroblasts and perivascular cells during zebrafish heart regeneration. *Dev. Biol.* **370**, 173–186. doi:10.1016/j.ydbio.2012.07.007
- González-Rosa, J. M., Burns, C. E. and Burns, C. G. (2017). Zebrafish heart regeneration: 15 years of discoveries. *Regeneration (Oxf)* **4**, 105–123. doi:10.1002/reg2.83
- Grandclement, C., Pallandre, J. R., Valmary Degano, S., Viel, E., Bouard, A., Bolland, J., Rémy-Martin, J.-P., Simon, B., Rouleau, A., Boireau, W. et al. (2011). Neuropilin-2 expression promotes TGF-beta1-mediated epithelial to mesenchymal transition in colorectal cancer cells. *PLoS ONE* **6**, e20444. doi:10.1371/journal.pone.0020444
- Gu, C., Rodriguez, E. R., Reimert, D. V., Shu, T., Fritzsche, B., Richards, L. J., Kolodkin, A. L. and Ginty, D. D. (2003). Neuropilin-1 conveys semaphorin and VEGF signaling during neural and cardiovascular development. *Dev. Cell* **5**, 45–57. doi:10.1016/S1534-5807(03)00169-2
- Jopling, C., Sleep, E., Raya, M., Martí, M., Raya, A. and Belmonte, J. C. I. (2010). Zebrafish heart regeneration occurs by cardiomyocyte dedifferentiation and proliferation. *Nature* **464**, 606–609. doi:10.1038/nature08899
- Kawasaki, T., Kitsukawa, T., Bekku, Y., Matsuda, Y., Sanbo, M., Yagi, T. and Fujisawa, H. (1999). A requirement for neuropilin-1 in embryonic vessel formation. *Development* **126**, 4895–4902.
- Kikuchi, K., Holdway, J. E., Werdich, A. A., Anderson, R. M., Fang, Y., Egnaczyk, G. F., Evans, T., Macrae, C. A., Stainier, D. Y. R. and Poss, K. D. (2010). Primary contribution to zebrafish heart regeneration by *gata4*(+) cardiomyocytes. *Nature* **464**, 601–605. doi:10.1038/nature08804
- Kikuchi, K., Holdway, J. E., Major, R. J., Blum, N., Dahn, R. D., Begemann, G. and Poss, K. D. (2011). Retinoic acid production by endocardium and epicardium is an injury response essential for zebrafish heart regeneration. *Dev. Cell* **20**, 397–404. doi:10.1016/j.devcel.2011.01.010
- Kim, J., Wu, Q., Zhang, Y., Wiens, K. M., Huang, Y., Rubin, N., Shimada, H., Handin, R. I., Chao, M. Y., Tuan, T.-L. et al. (2010). PDGF signaling is required for epicardial function and blood vessel formation in regenerating zebrafish hearts. *Proc. Natl. Acad. Sci. USA* **107**, 17206–17210. doi:10.1073/pnas.0915016107

- Kim, J., Rubin, N., Huang, Y., Tuan, T.-L. and Lien, C.-L. (2012). In vitro culture of epicardial cells from adult zebrafish heart on a fibrin matrix. *Nat. Protoc.* **7**, 247-255. doi:10.1038/nprot.2011.440
- Kitsukawa, T., Shimizu, M., Sanbo, M., Hirata, T., Taniguchi, M., Bekku, Y., Yagi, T. and Fujisawa, H. (1997). Neuropilin-semaphorin III/D-mediated chemorepulsive signals play a crucial role in peripheral nerve projection in mice. *Neuron* **19**, 995-1005. doi:10.1016/S0896-6273(00)80392-X
- Kofler, N. and Simons, M. (2016). The expanding role of neuropilin: regulation of transforming growth factor-beta and platelet-derived growth factor signaling in the vasculature. *Curr. Opin Hematol.* **23**, 260-267. doi:10.1097/MOH.0000000000000233
- Kok, F. O., Shin, M., Ni, C.-W., Gupta, A., Grosse, A. S., van Impel, A., Kirchmaier, B. C., Peterson-Maduro, J., Kourkoulis, G., Male, I. et al. (2015). Reverse genetic screening reveals poor correlation between morpholino-induced and mutant phenotypes in zebrafish. *Dev. Cell* **32**, 97-108. doi:10.1016/j.devcel.2014.11.018
- Lee, P., Goishi, K., Davidson, A. J., Mannix, R., Zon, L. and Klagsbrun, M. (2002). Neuropilin-1 is required for vascular development and is a mediator of VEGF-dependent angiogenesis in zebrafish. *Proc. Natl. Acad. Sci. USA* **99**, 10470-10475. doi:10.1073/pnas.162366299
- Lepilina, A., Coon, A. N., Kikuchi, K., Holdway, J. E., Roberts, R. W., Burns, C. G. and Poss, K. D. (2006). A dynamic epicardial injury response supports progenitor cell activity during zebrafish heart regeneration. *Cell* **127**, 607-619. doi:10.1016/j.cell.2006.08.052
- Lien, C.-L., Schebesta, M., Makino, S., Weber, G. J. and Keating, M. T. (2006). Gene expression analysis of zebrafish heart regeneration. *PLoS Biol.* **4**, e260. doi:10.1371/journal.pbio.0040260
- Marín-Juez, R., Marass, M., Gauvrit, S., Rossi, A., Lai, S.-L., Materna, S. C., Black, B. L. and Stainier, D. Y. R. (2016). Fast revascularization of the injured area is essential to support zebrafish heart regeneration. *Proc. Natl. Acad. Sci. USA* **113**, 11237-11242. doi:10.1073/pnas.1605431113
- Martyn, U. and Schulte-Merker, S. (2004). Zebrafish neuropilins are differentially expressed and interact with vascular endothelial growth factor during embryonic vascular development. *Dev. Dyn.* **231**, 33-42. doi:10.1002/dvdy.20048
- Masters, M. and Riley, P. R. (2014). The epicardium signals the way towards heart regeneration. *Stem Cell Res.* **13**, 683-692. doi:10.1016/j.scr.2014.04.007
- Pellet-Many, C., Frankel, P., Jia, H. and Zachary, I. (2008). Neuropilins: structure, function and role in disease. *Biochem. J.* **411**, 211-226. doi:10.1042/BJ20071639
- Pellet-Many, C., Frankel, P., Evans, I. M., Herzog, B., Jünemann-Ramírez, M. and Zachary, I. C. (2011). Neuropilin-1 mediates PDGF stimulation of vascular smooth muscle cell migration and signalling via p130Cas. *Biochem. J.* **435**, 609-618. doi:10.1042/BJ20100580
- Pellet-Many, C., Mehta, V., Fields, L., Mahmoud, M., Lowe, V., Evans, I., Ruivo, J. and Zachary, I. (2015). Neuropilins 1 and 2 mediate neointimal hyperplasia and re-endothelialization following arterial injury. *Cardiovasc. Res.* **108**, 288-298. doi:10.1093/cvr/cvv229
- Peralta, M., González-Rosa, J. M., Marques, I. J. and Mercader, N. (2014). The epicardium in the embryonic and adult zebrafish. *J. Dev. Biol.* **2**, 101-116. doi:10.3390/jdb2020101
- Porrello, E. R., Mahmoud, A. I., Simpson, E., Hill, J. A., Richardson, J. A., Olson, E. N. and Sadek, H. A. (2011). Transient regenerative potential of the neonatal mouse heart. *Science* **331**, 1078-1080. doi:10.1126/science.1200708
- Poss, K. D., Wilson, L. G. and Keating, M. T. (2002). Heart regeneration in zebrafish. *Science* **298**, 2188-2190. doi:10.1126/science.1077857
- Roger, V. L. (2013). Epidemiology of heart failure. *Circ. Res.* **113**, 646-659. doi:10.1161/CIRCRESAHA.113.300268
- Schnabel, K., Wu, C.-C., Kurth, T. and Weidinger, G. (2011). Regeneration of cryoinjury induced necrotic heart lesions in zebrafish is associated with epicardial activation and cardiomyocyte proliferation. *PLoS ONE* **6**, e18503. doi:10.1371/journal.pone.0018503
- Soker, S., Takashima, S., Miao, H. Q., Neufeld, G. and Klagsbrun, M. (1998). Neuropilin-1 is expressed by endothelial and tumor cells as an isoform-specific receptor for vascular endothelial growth factor. *Cell* **92**, 735-745. doi:10.1016/S0092-8674(00)81402-6
- Taku, A. A., Marcaccio, C. L., Ye, W., Krause, G. J. and Raper, J. A. (2016). Attractant and repellent cues cooperate in guiding a subset of olfactory sensory axons to a well-defined protoglomerular target. *Development* **143**, 123-132. doi:10.1242/dev.127985
- van Wijck, B., Gunst, Q. D., Moorman, A. F. M. and van den Hoff, M. J. B. (2012). Cardiac regeneration from activated epicardium. *PLoS ONE* **7**, e44692. doi:10.1371/journal.pone.0044692
- Vieira, J. M., Norman, S., Villa del Campo, C., Cahill, T. J., Barnette, D. N., Gunadasa-Rohling, M., Johnson, L. A., Greaves, D. R., Carr, C. A., Jackson, D. G. et al. (2018). The cardiac lymphatic system stimulates resolution of inflammation following myocardial infarction. *J. Clin. Invest.* **128**, 3402-3412. doi:10.1172/JCI97192
- von Gise, A., Zhou, B., Honor, L. B., Ma, Q., Petryk, A. and Pu, W. T. (2011). WT1 regulates epicardial epithelial to mesenchymal transition through beta-catenin and retinoic acid signaling pathways. *Dev. Biol.* **356**, 421-431. doi:10.1016/j.ydbio.2011.05.668
- Wada, A. M., Smith, T. K., Osler, M. E., Reese, D. E. and Bader, D. M. (2003). Epicardial/Mesothelial cell line retains vasculogenic potential of embryonic epicardium. *Circ. Res.* **92**, 525-531. doi:10.1161/01.RES.0000060484.11032.0B
- Wang, L., Zeng, H., Wang, P., Soker, S. and Mukhopadhyay, D. (2003). Neuropilin-1-mediated vascular permeability factor/vascular endothelial growth factor-dependent endothelial cell migration. *J. Biol. Chem.* **278**, 48848-48860. doi:10.1074/jbc.M310047200
- West, D. C., Rees, C. G., Duchesne, L., Patey, S. J., Terry, C. J., Turnbull, J. E., Delehedde, M., Heegaard, C. W., Allain, F., Vanpouille, C. et al. (2005). Interactions of multiple heparin binding growth factors with neuropilin-1 and potentiation of the activity of fibroblast growth factor-2. *J. Biol. Chem.* **280**, 13457-13464. doi:10.1074/jbc.M410924200
- Yu, H.-H., Houart, C. and Moens, C. B. (2004). Cloning and embryonic expression of zebrafish neuropilin genes. *Gene Expr. Patterns* **4**, 371-378. doi:10.1016/j.modgep.2004.01.011
- Zamora, M., Manner, J. and Ruiz-Lozano, P. (2007). Epicardium-derived progenitor cells require beta-catenin for coronary artery formation. *Proc. Natl. Acad. Sci. USA* **104**, 18109-18114. doi:10.1073/pnas.0702415104
- Zhou, B. and Pu, W. T. (2011). Epicardial epithelial-to-mesenchymal transition in injured heart. *J. Cell. Mol. Med.* **15**, 2781-2783. doi:10.1111/j.1582-4934.2011.01450.x

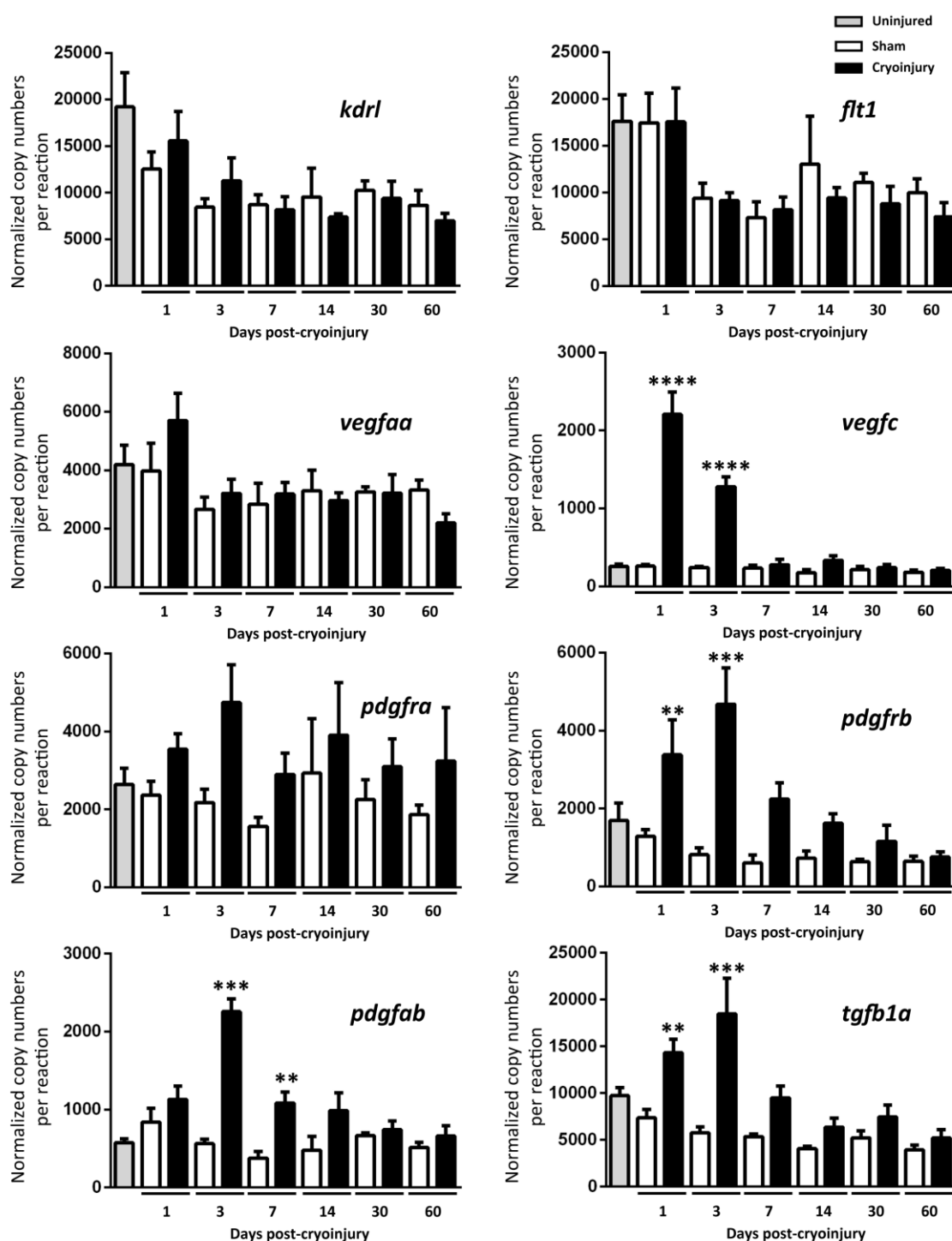


Figure S1 Gene expression of vascular endothelial growth factors (*vegfa*), platelet-derived growth factor (*pdgfa*) and transforming growth factor (*tgfa*) and their receptors in adult zebrafish cryoinjured ventricles.

Absolute quantitative PCR analysis 1, 3, 7, 14, 30, and 60 days following cryoinjury or sham surgery of zebrafish ventricles. Basal expression was evaluated in uninjured hearts. *Vegf* receptors *kdrl* and *flt1* and *vegfa* isoforms (*vegfaa* and *vegfc*) mRNA levels

were assessed to evaluate expression of genes associated with angiogenesis. *Pdgf* receptors *pdgfra* (*pdgfr* α) and *pdgfrb* (*pdgfr* β), additional to *pdgf* (*pdgfab*) and *tgf* (*tgfb1a*) gene expression were measured to evaluate expression of genes associated epithelial-to-mesenchymal transition. Bars represent means of normalized copy numbers per reaction \pm S.E.M, ** $p < 0.01$, *** $p < 0.005$, **** $p < 0.001$ (one-way ANOVA with Sidak's *post hoc* test for multiple comparisons of $n = 4-5$ with each n being a pool of 5 ventricles).

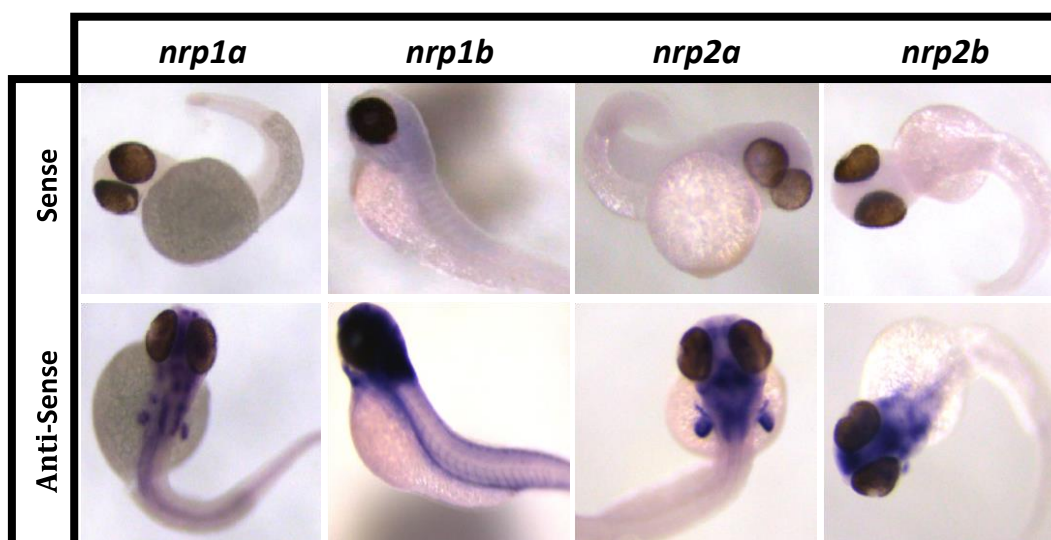


Figure S2 *nrp* riboprobes validation.

In situ hybridization of TraNac transgenic zebrafish embryos 48 hours post fertilization (hpf) with *nrp* sense riboprobes (**upper row**) and *nrp* anti-sense riboprobes (**lower row**). Anti-sense riboprobes differential staining patterns were compared to previous reports (43) to confirm specific *nrp* isoform detection. All neuropilin isoforms are observed in the brain with additional differential expression patterns observed between different isoforms. *Nrp1a* is observed in the fin buds and otic vesicles, *nrp1b* is expressed in the dorsal aorta and intersegmental vessels, *nrp2a* is observed in the hind brain and fin buds, whereas *nrp2b* is largely restricted to the brain and hind brain, $n \geq 8$.

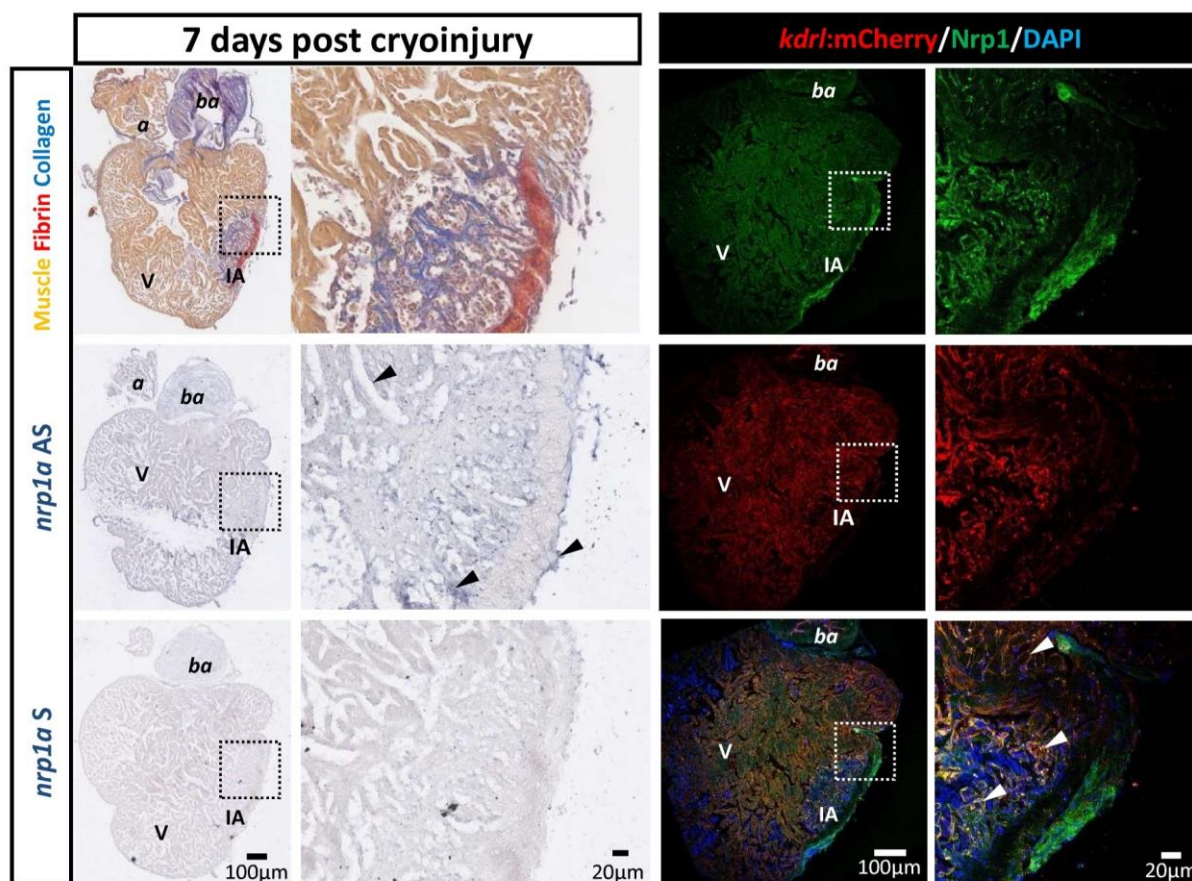


Figure S3 Nrp1 is expressed by the endocardium.

AFOG staining (**upper left panels**), *in situ* hybridization (ISH) (**middle and lower left panels**) and immunofluorescence (**two right columns**) of *tg(kdr:mCherry)^{s896}* zebrafish heart 7 days post cryoinjury (dpi). AFOG staining gives reference to cryoinjury location and tissue composition. ISH of *nrp1a* anti-sense riboprobe (*nrp1a* AS) (**middle left panels**) and negative control sense (*nrp1a* S) riboprobe (**lower left panels**), signal is observed as a dark blue stain within the section, black arrows indicate mRNA expression. *kdr* expression by viable endocardium is immunolabeled with anti-mCherry antibody (red) (**middle right panels**) and Nrp1-expressing cells are labelled in green (**upper right panels**). Overlay of the two colors is displayed with DAPI nuclei staining (**lower right panels**). White arrows indicate regions of colocalization. Dotted boxes highlight magnified regions. V– ventricle, *ba*– *bulbus arteriosus*, *a*– atrium, IA– injured area ($n = 2$).

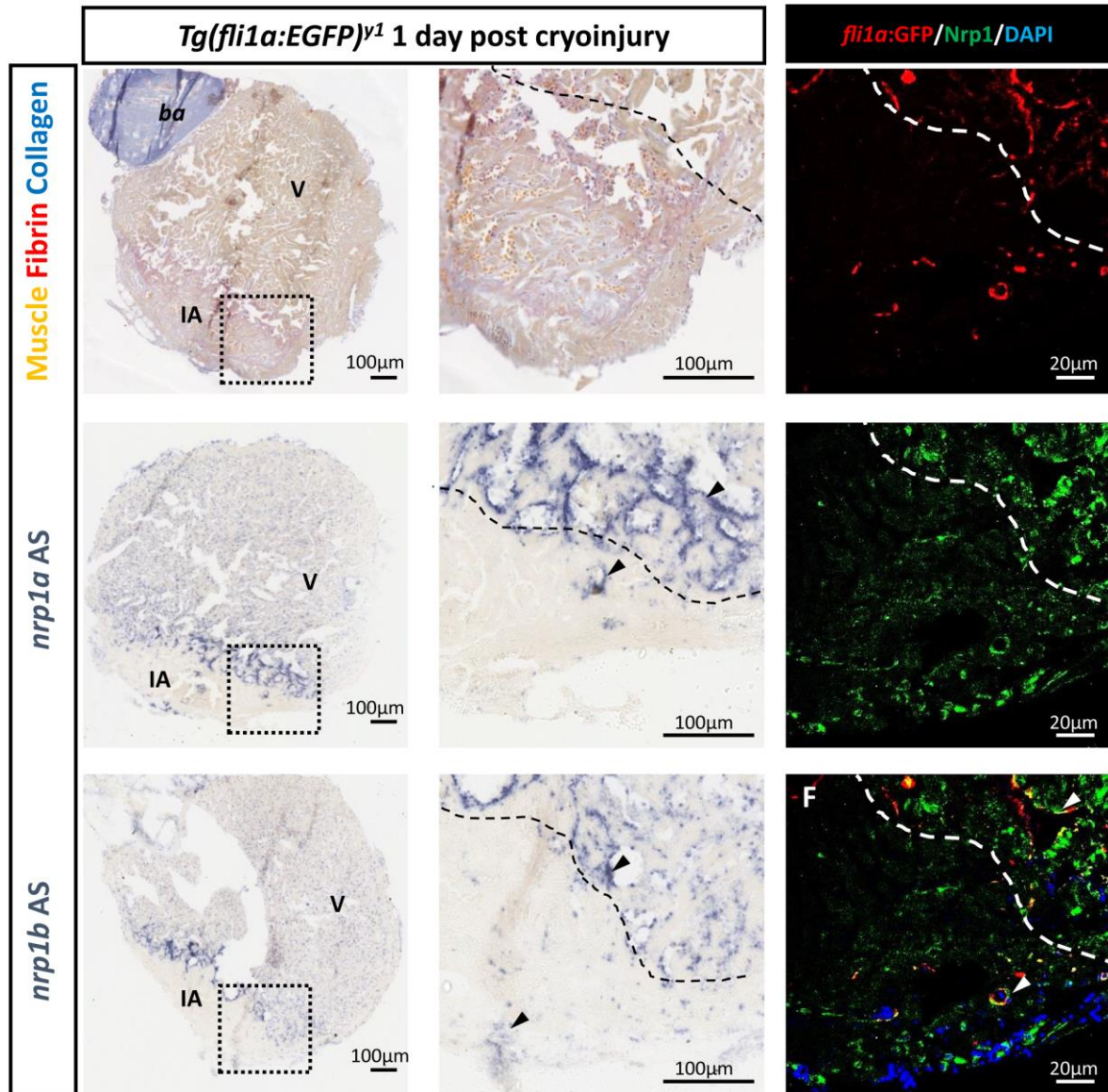


Figure S4 Nrp1 is expressed by early neovasculature in the cryoinjured lesion of *tg(fli1a:EGFP)^{y1}* zebrafish heart 1 day post cryoinjury.

AFOG staining (**upper left**) identifies cryoinjured lesion. *Nrp1a* (**middle left**) and *nrp1b* (**lower left**) mRNA localization is detected with *in situ* hybridization, black arrows indicate mRNA expression within the injury and at the injury/healthy myocardium border. Immunofluorescence imaging was used to locate *fli1a:EGFP* positive cells expressed by viable endothelium and endocardium (red) (**upper right**) and Nrp1-expressing cells (green) (**middle right**). Overlay of the two colors are displayed with DAPI nuclei staining (**lower right pane**), white arrows indicate areas of colocalization. Dotted boxes highlight magnified regions. Dashed lines define injury interface. V– ventricle, *ba*– *bulbus arteriosus*, IA– injured area, $n = 3$.

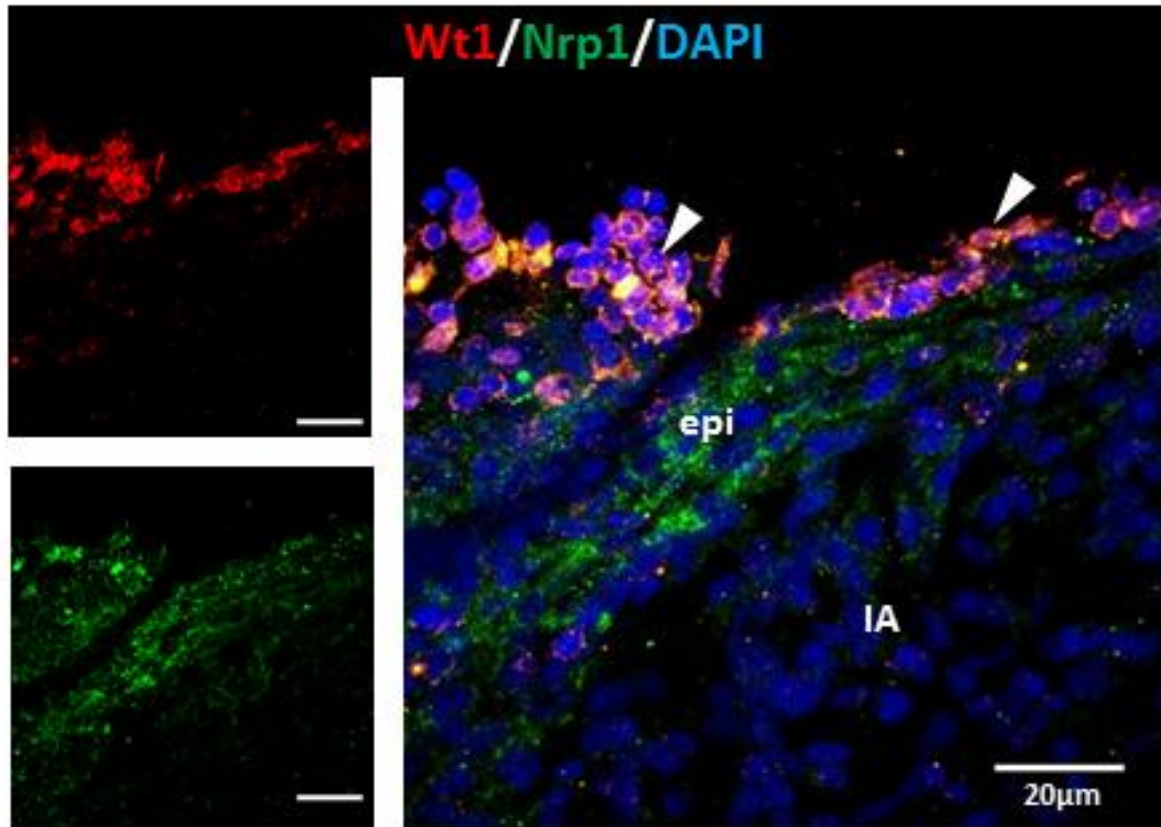


Figure S5 Wt1-positive epicardial cells express Nrp1.

Immunofluorescence of Wild-Type adult zebrafish heart 3 days post cryoinjury (dpci). Activated epicardial cells were identified with Wt1 antibody (red) and assessed for Nrp1 expression (green). White arrows indicate regions of colocalization. Scale bars = 20µm. IA– injured area, epi– epicardium ($n = 2$).

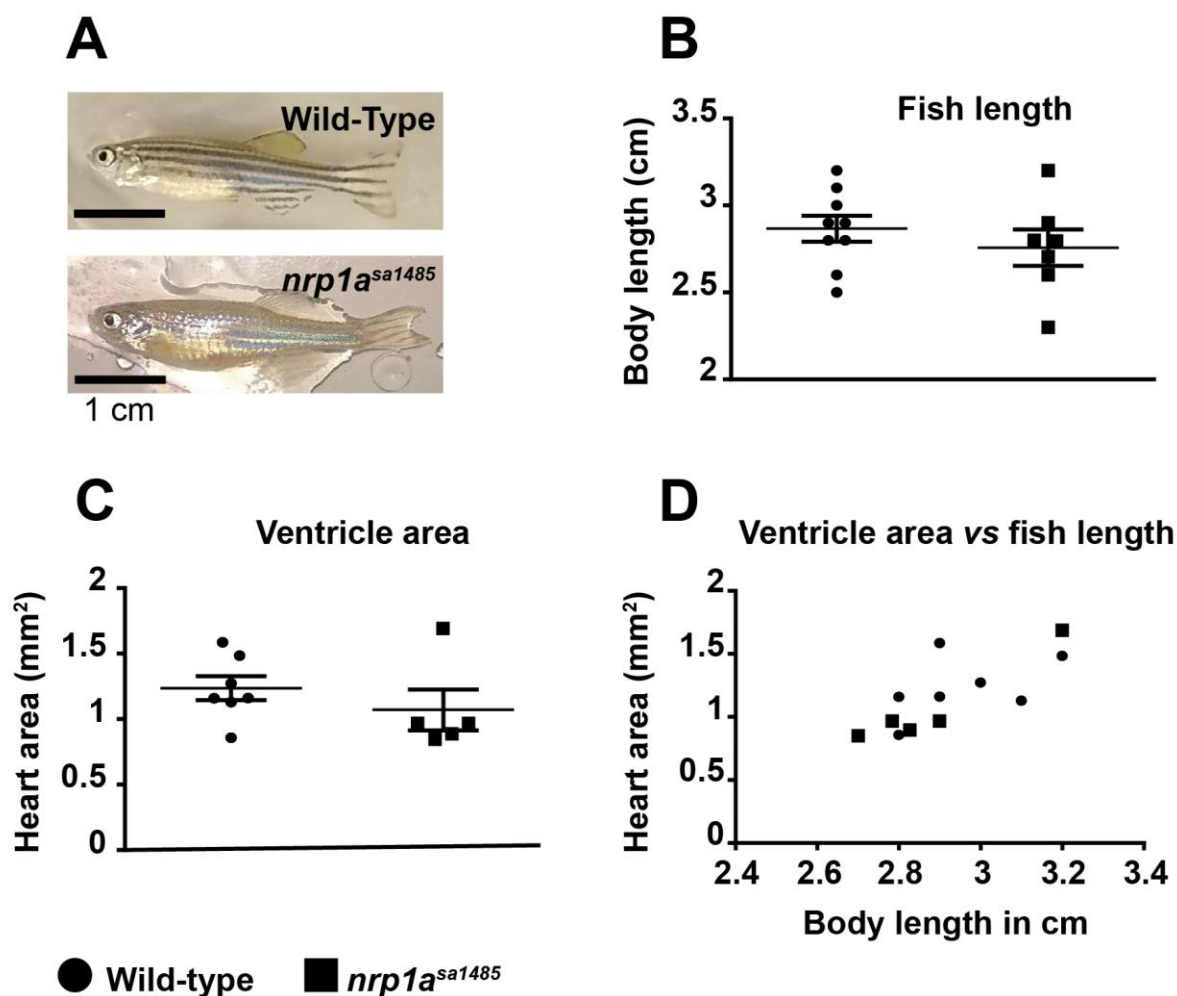


Figure S6 *nrp1a*^{sa1485} mutant fish characterization

(A) Representative picture of Wild-Type (upper panel) and *nrp1a*^{sa1485} mutant zebrafish (lower panel), scale bar 1 cm. The body length (B), and heart size (C) of age matched Wild-Type (black dots) and *nrp1a*^{sa1485} mutant (black squares) zebrafish were measured and compared (two-tailed *t*-test of $n \geq 5$, $p > 0.05$). (D) Scatter graph representing the values of body length to heart size ratio. Values are displayed as individual measurements of fish indicated as black dots (Wild-Type) or squares (*nrp1a*^{sa1485}).

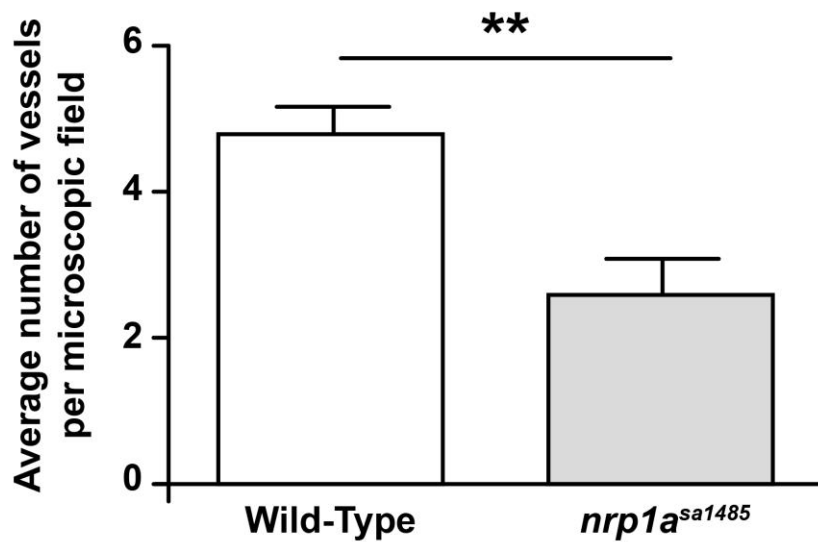
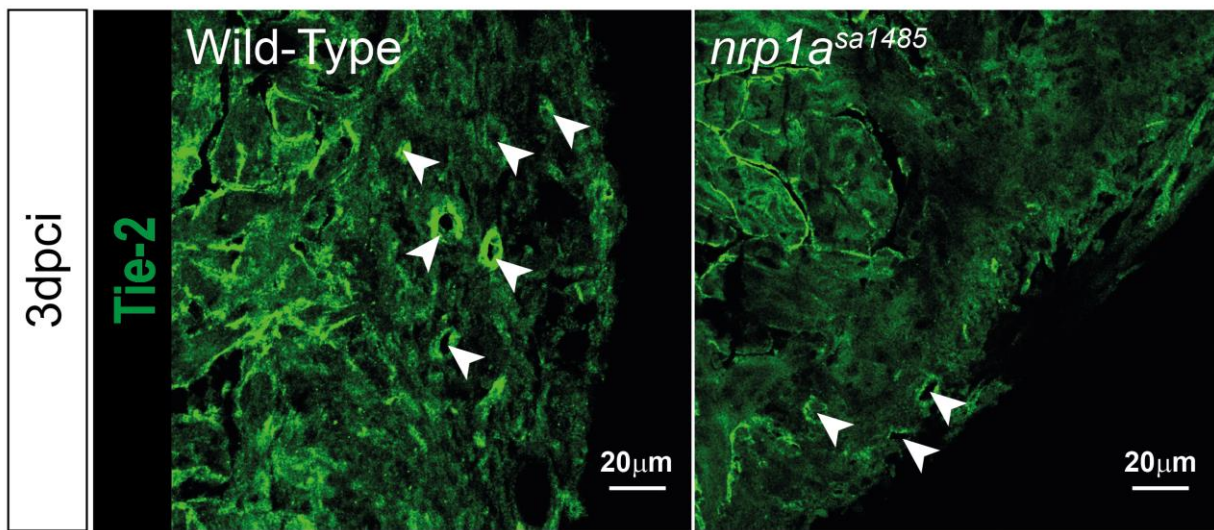


Figure S7 Neovascularization of the cryoinjured area is impaired in *nrp1a*^{sa1485} fish.

Tie2 immunostaining of Wild-Type (top left) and *nrp1a*^{sa1485} (top right) hearts 3 days post cryoinjury. Bars represent average numbers of newly formed vessels per microscopic field (32625 μm²) within the injured area ± S.E.M, samples were quantified at least at 3 levels across the whole hearts (two-tailed *t*-test of *n* = 6, ** *p* < 0.01).

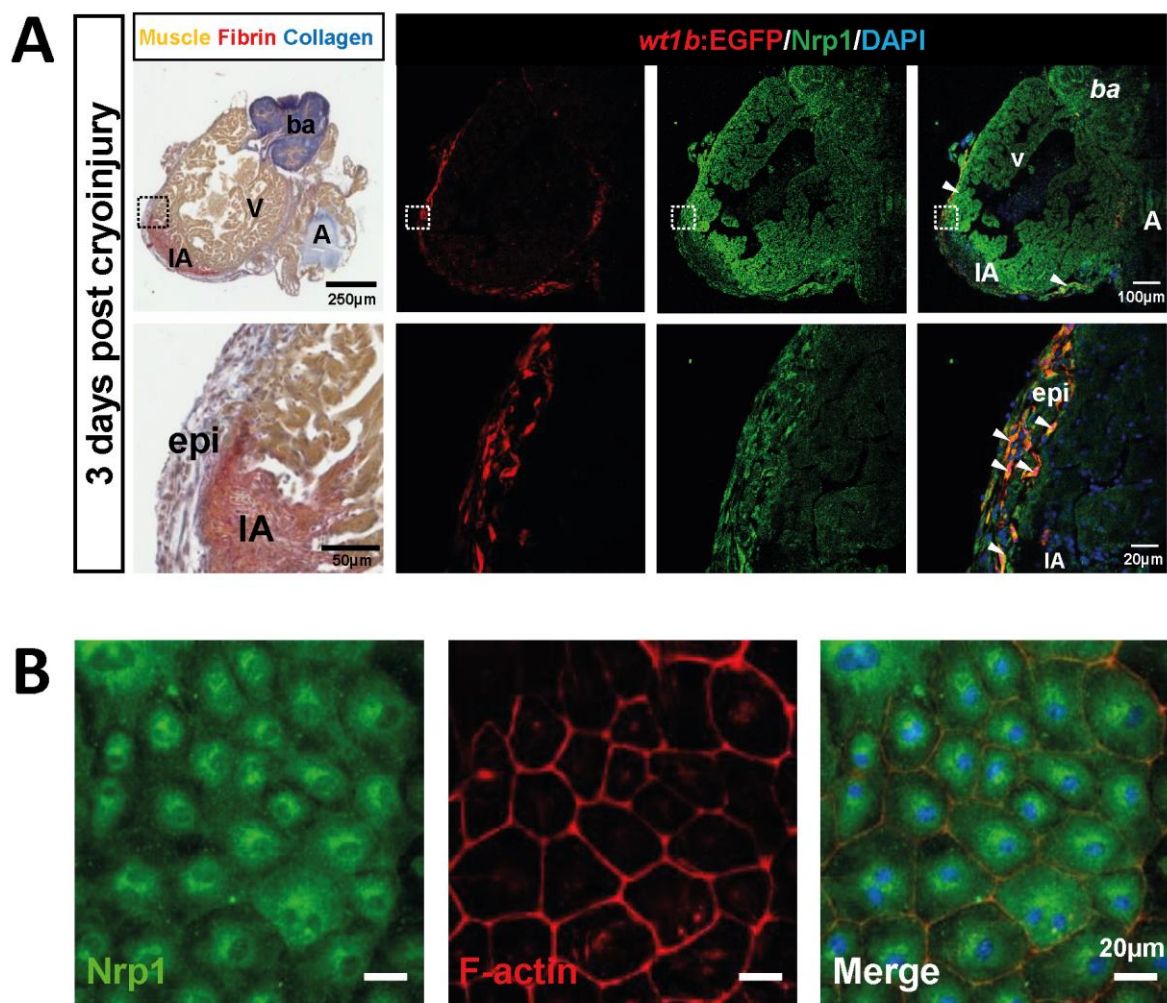


Figure S8 Epicardial cells express Nrp1 *in vivo* and *in vitro*.

(A) Serial sections of *tg(wt1b:EGFP)^{li1}* adult zebrafish heart 3 dpci stained with AFOG for lesion location and immunostained for GFP (red), Nrp1 (green) and DAPI (right panels). Dotted boxes indicate magnified region in panels below. White arrows identify cells co-expressing GFP and Nrp1. V– ventricle, ba– *bulbus arteriosus*, A– atrium, IA– injured area, epi– epicardium ($n = 3$). **(B)** Wild-Type ventricle apices were collected 5 dpci and cultured *in vitro* for 7 days and epicardial outgrowths immunostained for Nrp1. All epicardial cells of the explant were Nrp1 positive. Phalloidin conjugated to Alexa-555 was used to identify F-actin and highlight cellular tight junctions and DAPI staining applied to located individual cells. Scale bar 20 μm ($n = 4$).

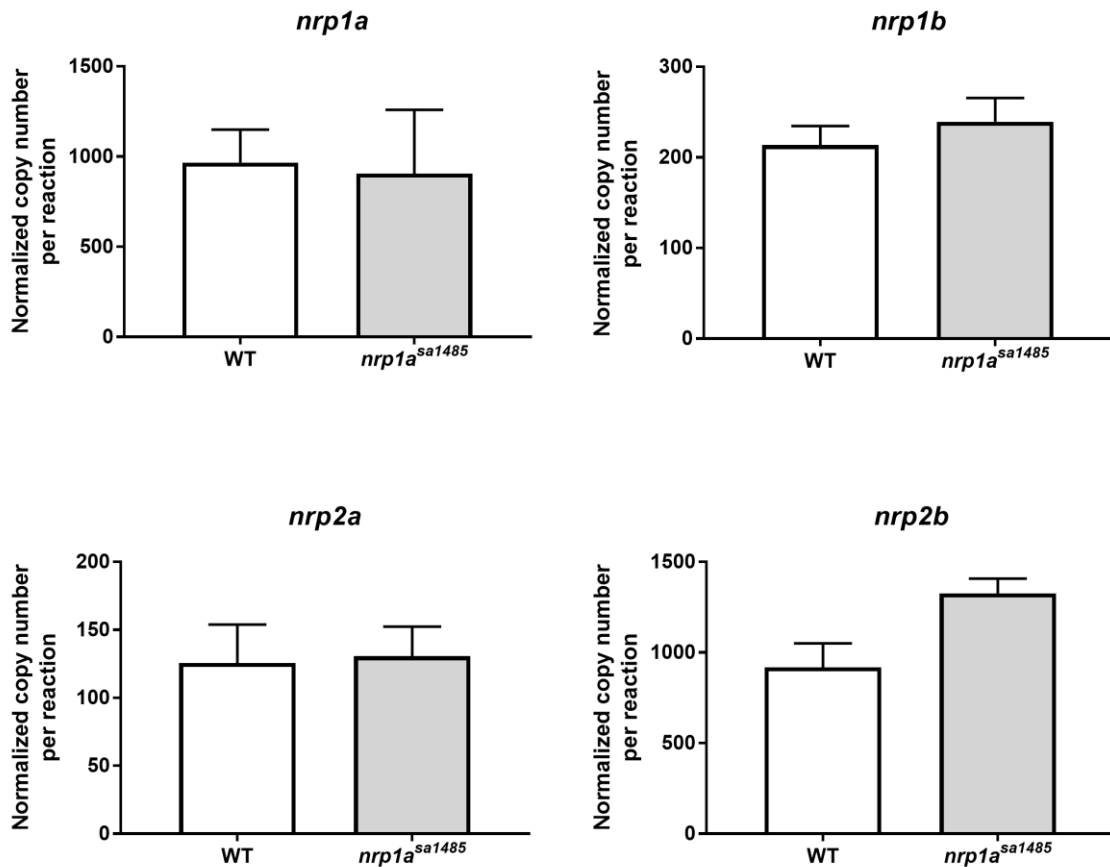


Figure S9 Gene expression of all neuropilin isoforms remains unchanged in *nrp1a^{sa1485}* fish after cryoinjury.

Absolute quantitative PCR analysis at 3 days following cryoinjury of Wild-Type or *nrp1a^{sa1485}* zebrafish ventricles. Bars represent means of normalized copy numbers per reaction \pm S.E.M, (two-tailed *t*-tests of $n=6$ for Wild-Type and $n=4$ for *nrp1a^{sa1485}* fish, each n is one heart, $p>0.05$).

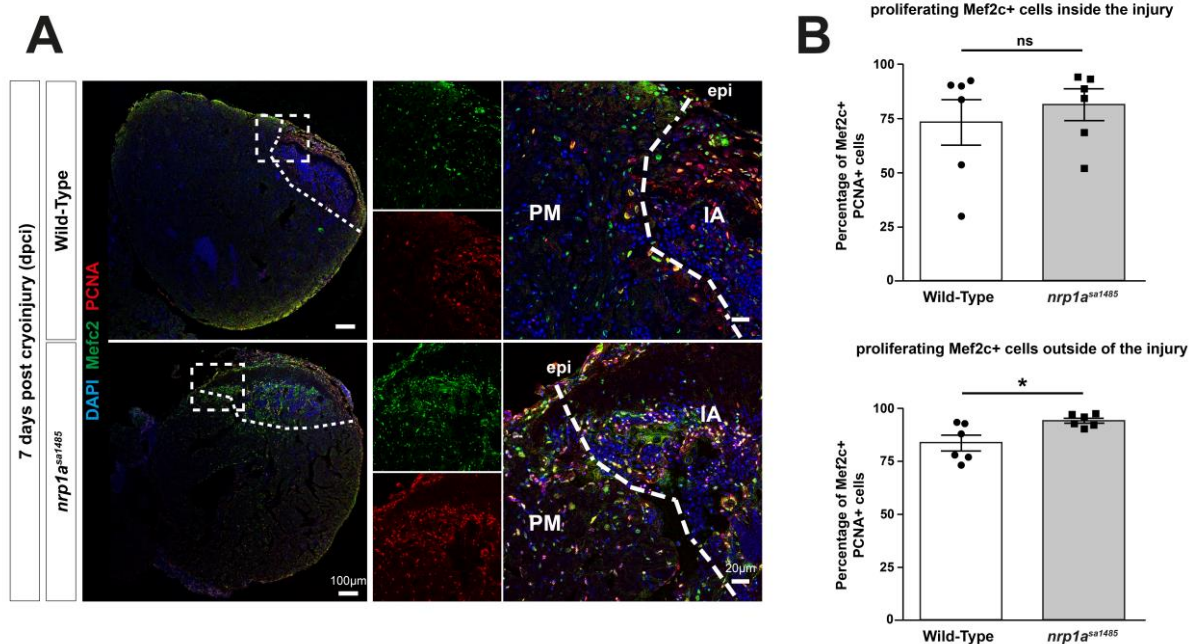


Figure S10 Cardiomyocyte proliferation of *nrp1a^{sa1485}* mutant is not affected following cryoinjury.

Sections of Wild-Type and *nrp1a^{sa1485}* mutant cryoinjured hearts (7 dpci) were examined by immunofluorescent staining for Mef2c and PCNA and counterstained with DAPI. The percentage of PCNA+ cardiomyocytes (i.e., also Mef2c-positive) inside the injury as well as at the injury periphery were quantified. Data points represent average values of individual hearts, obtained from 2-3 sections per heart, (two-tailed *t*-test of $n=6$, $p=0.542$ inside the injury, Mann-Whitney non parametric test of $n=6$, $p=0.065$ in the periphery). PM – peripheral myocardium to the injury, IA – injured area, epi – epicardium

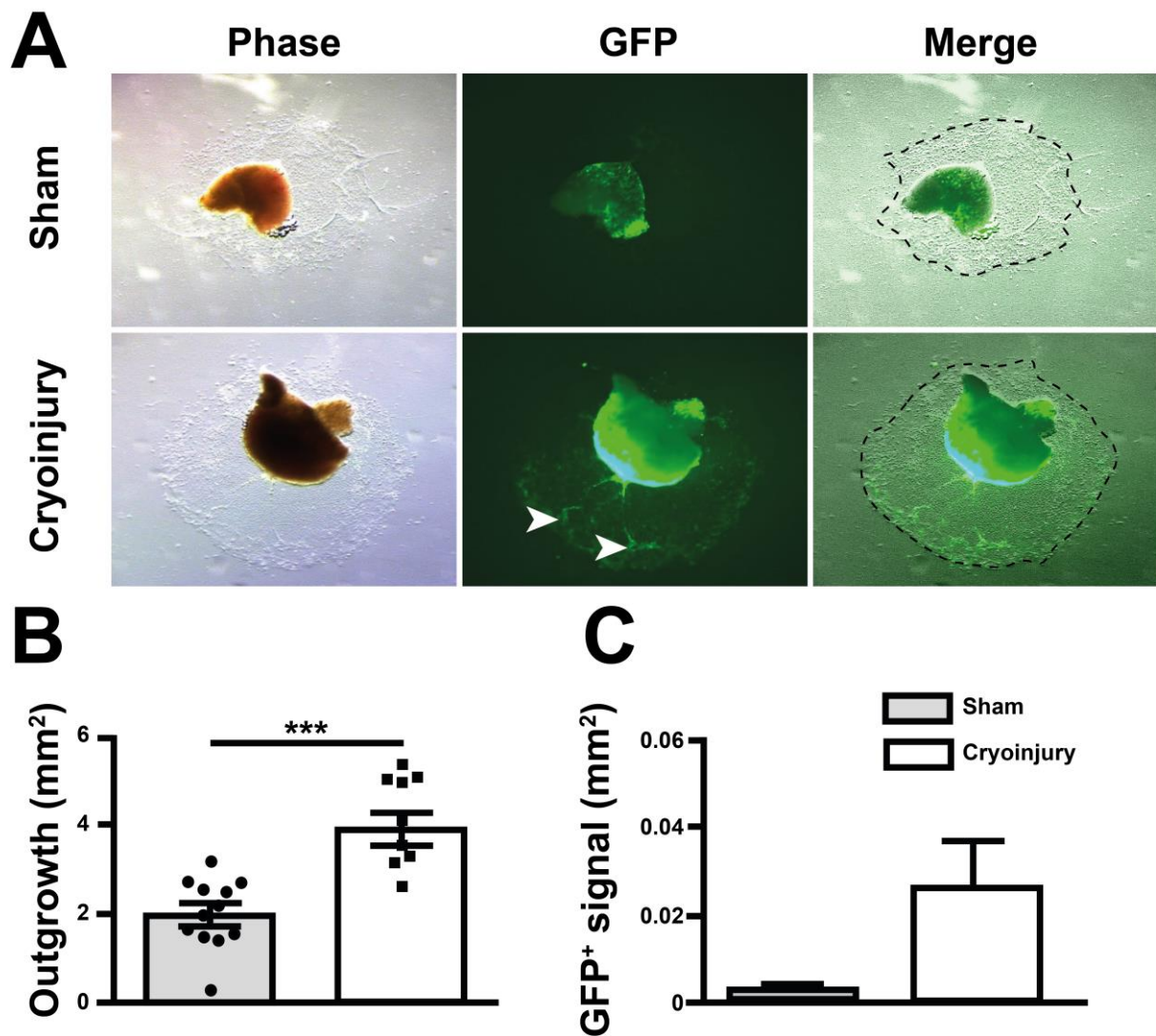


Figure S11 Cryoinjury induces epicardial activation and expansion in heart explants.

The apices of *tg(wt1b:EGFP)^{li1}* zebrafish ventricles were collected 5 days post sham surgery or cryoinjury and cultured on fibrin gels for 7 days. **(A)** Explants were imaged using a stereomicroscope under phase contrast and green-fluorescence, then overlaid to visualize GFP-positive epicardial outgrowth (white arrows), scale bar 500 μ m. **(B)** Epicardial outgrowths from sham (white bar) and cryoinjury (grey bar) surgeries were quantified. Results are presented as mean outgrowth in mm² \pm S.E.M (two-tailed *t*-test of *n* = 12 sham and *n* = 10 cryoinjury, ****p*=0.0003). **(C)** GFP+ signal in the epicardial outgrowth was measured for sham (white bar) and cryoinjury (grey bar) surgeries. Results are presented as mean GFP+ signal area in mm² \pm S.E.M (two-tailed *t*-test of *n* = 4, *p*=0.0713).

Gene	Name	Accession Number	Primer Sequence 5'-3'
<i>rpl13a</i>	Ribosomal protein L 13A	NM_212784	Fwd gtctgaaacccacacgcaaat Rev cgttctttcagcctgcttagt
<i>eef1a1a</i>	Eukaryotic translation elongation factor 1a	NM_200009	Fwd ctctctgggtcgtttgct Rev tatgtgtctctggagtggca
<i>gapdh</i>	Glyceraldehyde 3-phosphate dehydrogenase	NM_001115114	Fwd ttctgagctcaatggcaagc Rev agacggactgtcagatccaca
<i>nrp1a</i>	Neuropilin 1a	NM_001040326 & NM_181497	Fwd ctccaacaaaccctaccaggt Rev tcggtgatgtccaccatgattc
<i>nrp1b</i>	Neuropilin 1b	AY493415	Fwd gaccaaagcagatggagggaa Rev catctctgtattctctggatcttgc
<i>nrp2a</i>	Neuropilin 2a	NM_212965	Fwd gattctgacttcagctgggtatg Rev cgatgtacaggtagttcccaaa
<i>nrp2b</i>	Neuropilin 2b	NM_212966	Fwd cagcattgagcttgagcagt Rev tcaggctctcgctcagtcac
<i>kdrl</i>	Kinase insert domain receptor like	NM_131472	Fwd ccttgagacgcagatgaatcc Rev ctgctgtatccaccctggct
<i>flt1</i>	Fms-related tyrosine kinase 1	NM_001014829 & NM_001257153	Fwd aactcacagaccagtgaacaaga Rev ttagccttctgtgggtatgtcca
<i>vegfaa</i>	Vascular endothelial growth factor Aa	NM_001190933	Fwd ccatctgtctgctgtaaaggct Rev gatgatgtctaccagcagctctc

vegfc	Vascular endothelial growth factor c	NM_205734	Fwd tgccatgcaggagcattcaga Rev gcctcctccgacctgtttc
tgfb1a	Transforming growth factor beta 1a	NM_212965	Fwd gctggctctcatttgacgtg Rev ctctgctgtctagccctga
pdgfra	Platelet-derived growth factor receptor alpha	NM_131459	Fwd tgataatctctacacaacgctgagt Rev ctcatagacatcactggacgcat
pdgfrb	Platelet-derived growth Factor receptor beta	NM_001190933	Fwd gctatcacaacaggactggttc Rev ctctgtgcgaaagtctggga
pdgfab	Platelet derived growth factor alpha b	NM_001076757	Fwd tgataatctctacacaacgctgagt Rev caggggtctgaggtaaagtc
aldh1a2	retinaldehyde dehydrogenase 2	NM031850	Fwd gcgatgacctccagtgaagttg Rev acctgccgctcacagaatcat

Table S1 RT-qPCR primers used for zebrafish gene expression analyses

Supplementary Materials and Methods:

Zebrafish husbandry, cryoinjury and sample collection

Procedures were performed in line with the Animals (Scientific Procedures) Act 1986, and husbandry was regulated by the Central University College London fish facility. Adult zebrafish between 6-18 months of age were used for the study. Wild-Type ABxTupLF (ABxTübingen-long fin) (Max-Planck, Tübingen, Germany) and *nrp1a*^{sa1485/sa1485} (Zebrafish Mutation Project, Sanger Center, Cambridge, UK) fish were used for *in vitro* culture, histological samples, RNA, and protein expression analysis. Additionally, the following transgenic fish were used for histological and *in vitro* preparations: *Tg(fli1a:EGFP)^{y1}* and *tg(kdrl:mCherry)^{s896}* to identify endocardial cells, *tg(wt1b:EGFP)^{li1}* to detect activated epicardial cells. TraNac zebrafish embryos (gift from Paul Frankel, University College London) were used for whole-mount *in situ* hybridization probe validation.

The cryoinjury procedure was carried out as described in (Gonzalez-Rosa and Mercader, 2012). Briefly, fish were anaesthetized and a small incision was made to expose the ventricle. A stainless steel probe (0.75 mm diameter), cooled in liquid nitrogen, was pressed onto the ventricle apex for 5 seconds. Sham surgeries were performed as above, with the absence of probe application.

For RNA extraction, ventricles were rinsed briefly in PBS and stored at -20°C in RNAlater® stabilization reagent (Qiagen). For protein extraction, ventricles were snap frozen in liquid nitrogen and stored at -80°C until processing. For histological preparations, the entire heart (atrium, ventricle and *bulbus arteriosus*) was kept intact and placed in PBS/0.1 M KCL to arrest heart in diastole before fixing with 4% (wt/vol) paraformaldehyde overnight at 4°C. After fixation, hearts were rinsed several times in PBS, dehydrated in graded concentrations of ethanol solutions and embedded in

paraffin wax. Sections were cut in serial sections at 10 µm to slides. Sections used for Acid Fuchsin Orange G (AFOG) staining and immunohistochemistry were mounted to Superfrost® Plus slides and stored at room temperature, while sections prepared for *in situ* hybridization were mounted to Superfrost® ultra plus (both Thermo Fisher Scientific) and stored at -80°C for *in situ* hybridization procedures. For whole-mount *in situ* preparations, embryos were collected 48 hours post fertilization and fixed with 4% (wt/vol) paraformaldehyde overnight at 4°C. The following day, embryos were rinsed several times with PBS, dechorionated, and stored in 100% methanol at -20°C until processing.

RT-qPCR

Five ventricles from corresponding time points and treatments were pooled for RNA extraction and homogenized in lysis buffer (Qiagen) in 1.4mm ceramic bead-containing tubes and mechanically disrupted in a Minilys homogenizer (Peqlab). Homogenates were passed through a QIAshredder spin column (Qiagen) then total RNA was extracted using the RNeasy Mini Kit (Qiagen). The quantity and purity of RNA were evaluated using a NanoDrop 2000 spectrophotometer (Thermo Fisher Scientific) and RNA integrity was assessed with a Bioanalyzer (Agilent). 250-500 ng of total RNA was reverse transcribed using the QuantiTect® Reverse Transcription Kit (Qiagen).

All primers (see table S1) and standards were purchased from qStandard: Absolute RT-qPCR values were measured using Brilliant III Ultra-Fast QPCR Master Mix (Agilent Technologies Inc.) and the Rotor-Gene PCR thermocycler (Qiagen). Values were normalized using a normalization factor generated using GeNorm software from the following three reference genes: *gapdh*, *rpl13a* and *eef1a1a* to calculate the expression of the genes of interest.

Immunofluorescence

Whole heart sections were rehydrated in graded concentrations of ethanol solutions. Citrate buffer heat-induced antigen retrieval was performed (10 minutes) and samples were permeabilized in 0.5% Triton X-100 for 15 minutes followed by blocking for 1 hour at room temperature in blocking solution (PBS 0.1% Tween-20 (PBST) supplemented with 5% BSA and 10% donkey serum). Primary antibodies were diluted in blocking solution and incubated overnight at 4°C. The following antibodies were used for immunofluorescence: anti-Neuropilin 1, Abcam ab81321 (1:100) anti-WT1 6F-H2, Novus NB110-6001 (1:100); anti-GFP, Roche 11 814 460 001 (1:200); anti-Tropomyosin, sigma T2780 (1:100); anti-mCherry, Novus NBP1-96752 (1:100); anti-PCNA PC-10, Santa Cruz sc-56 (1:100); anti-ALDH2 (RALDH2), Genetex GTX101429 (1:100); anti-Mef2, biorbyt orb256682(1:100); normal rabbit IgG, alpha diagnostics 200009-1-200 (1:200); normal mouse IgG, Invitrogen 026502 (1:200). The following day, slides were washed in PBST and incubated with fluorescent secondary antibodies: anti-rabbit Alexa 488 and anti-mouse Alexa 555 (both Thermo Fisher Scientific, A31570 and A11034) for 1 hour at room temperature. Slides were washed with PBST and incubated in 1% (wt/vol) Sudan Black B in 70% ethanol for 15 minutes at room temperature to quench background fluorescence and rinsed 8 times rapidly with PBS before mounting with ProLong DAPI mounting medium (Thermo Fisher Scientific). Images were captured on the Leica TCS SPE1 confocal microscope system and processed using the publicly available ImageJ software.

AFOG staining

Deparaffinized and rehydrated sections were fixed in Bouins fixative (Thermo Fisher Scientific) for 2 hours at 60°C followed by overnight incubation at room temperature. The following day, slides were washed for 10 minutes in constant tap water stream. Nuclei were

stained with Weigert's iron hematoxylin (Amresco, Sigma-Aldrich), and treated for 5 minutes with 1% phosphomolybdic acid in ddH₂O (Sigma-Aldrich). Slides were then incubated in AFOG staining solution (5g Methyl Blue (Sigma), 10g Orange G (Sigma-Aldrich), 15g acid fuchsin (Acros organics) per litre of double distilled water (ddH₂O), pH=1.09) for 10 minutes and washed in ddH₂O 5 times. Slides were then rapidly dehydrated in a series of ethanol solutions of increasing concentrations to a final incubation in xylene and mounted for imaging in NanoZoomer automated slide scanner (Hamamatsu).

***In situ* hybridization**

Digoxigenin-labelled RNA (Roche) probe templates were generated from adult zebrafish heart cDNA, the primers used were as follows (5'-3'):

nrp1a fwd TACAGTGCCGCCTACTACAC, rev CACGCTTCCGAGTACGAGTT;

nrp1b fwd CAAAACCATGACACGCCAGA rev TGCCCTCACAGTTCACGATTT;

nrp2a fwd AGACCAGCACGACACAGAAA, rev GTGAGGGGTTTGGTGTGGTC;

nrp2b fwd ACCACCATTCTGACTGTC, rev GTGAGGGGTTTGGTGTGGTC.

Previously established probes, such as: *cmlc2*, *raldh2*, *wt1b* and *tbx18* (gift from Nadia Mercader, Universität Bern, Switzerland) were synthesized in a similar manner. Primers were used in a PCR reaction to amplify probe sequence region and amplicons cloned to pGEM®-T plasmid vectors. Each plasmid was used in two RNA polymerase reactions (either SP6 or T7) to generate the sense and the anti-sense probes.

After deparaffinization in xylene, sections were rehydrated, fixed with 4% (wt/vol) paraformaldehyde at room temperature for 10 minutes and digested with proteinase K (10µg/ml in PBS) at 37°C for 10 minutes. Sections were then post-fixed with 4% (wt/vol) paraformaldehyde for 5 minutes at room temperature, washed twice in PBS, and acetylated for 10 minutes with 0.25% acetic anhydride in 0.1 M triethanolamine (DEPC-treated), then

washed in PBS. Hybridization solution (50% deionised formamide, 10% dextran sulphate, 1X Denhardt's, 5X Saline-Sodium Citrate (SSC), 1 mg/ml yeast tRNA, 0.1% Tween 20) was placed on samples and incubated at 67°C for 2 hours in a humidifying chamber. Either anti-sense (AS) or sense (S) digoxigenin-labelled probes (0.5µg probe/ml) in hybridization solution were added to the samples overnight at 67°C in a humidifying chamber. Slides were washed at 67°C in graded salt solutions (5X SSC/50% formamide, 2X SSC/50% formamide, 2X SSC and 0.2X SSC) for 30 minutes per wash, then washed with malate buffer (100 mM maleic acid, 150 mM NaCl, pH7.5, 0.1% Tween 20) (MAB) 3 times, and blocked (MAB/ 2% Boehringer blocking reagent/10% sheep serum) at room temperature for 2 hours. Alkaline phosphatase-conjugated anti-digoxigenin antibody (Roche) was incubated on samples overnight at 4°C and, the following day, slides were washed with MAB and equilibrated in staining buffer (100 mM Tris pH9.5, 50 mM MgCl₂, 100 mM NaCl, 0.1% Tween 20). Gene detection by alkaline phosphatase/NBT/BCIP reaction (containing 5% polyvinyl alcohol) was carried out at 37°C in the dark until a signal was detected. Slides were fixed with 4% (wt/vol) paraformaldehyde before rapid dehydration in graded concentrations of ethanol solutions to xylene for imaging in NanoZoomer automated slide scanner (Hamamatsu).

Neuropilin probes were validated with whole-mount *in situ* hybridization of dechorionated embryos. Embryos were rehydrated in graded concentrations of methanol, permeabilized with proteinase K (10 µg/ml) at RT for 20 minutes and further fixed in 4% (wt/vol) paraformaldehyde. Hybridization buffer (50% formamide, 5X Saline-Sodium Citrate buffer (SSC), heparin (50 µg/ml), torula yeast tRNA (5 mg/ml), 0.1% Tween 20) was used to block embryos at 67°C for one hour. Probes were diluted to 0.5 µg probe/ml in the same hybridization buffer and denatured at 80°C for 3 minutes. Equilibrated embryos were then incubated in probe-containing hybridization solution at 67°C overnight. Similarly, detection was performed using alkaline phosphatase-conjugated anti-DIG antibodies (Roche).

Visualization was done using alkaline phosphatase substrate BM purple (Roche) in the dark at room temperature until a dark purple precipitant developed. Embryos were then post fixed with 4% (wt/vol) paraformaldehyde overnight at 4°C and stored in 80% glycerol/PBS for microscopic analysis.

***In vitro* epicardial cell culture (heart explants)**

Thrombin/fibrin reaction in Dulbecco's Modified Eagle Medium (DMEM, Thermo Fisher Scientific) was performed as described previously (Kim et al., 2012) to produce a fibrin gel matrix in either 24-well plates or Lab-Tek™II 4-chamber slides (Thermo Fisher Scientific). The apex of cryoinjured and sham-operated zebrafish hearts 5 days post-surgery were isolated and rinsed several times with HDMEM (23mM HEPES, 15mM NaCl in DMEM) to remove residual blood. One apex per well/chamber was placed firmly on set fibrin gel matrices, ensuring epicardial surface contact with the gel. Excess HDMEM was removed from heart tissue and left to adhere for 1 hour in a tissue culture incubator (28°C, 5% CO₂) before careful addition of DMEM supplemented with 0.5% fetal bovine serum (FBS), Normocin™ (invivoGen) and penicillin/streptomycin antibiotics (Sigma-Aldrich) into the wells or slide chambers. Medium was changed every 2 days and cells were cultured for 7 days before harvesting epicardial outgrowths for immunofluorescence imaging. For immunofluorescence analysis, heart tissue was discarded and cells were fixed in 4% (wt/vol) paraformaldehyde for 15 mins and permeabilized with 0.1% Triton X-100 for 10 mins before blocking in PBST (1% BSA, 10% donkey serum) at room temperature for 1 hour and incubated overnight at 4°C with primary antibody diluted in blocking solution. The antibodies used to stain epicardial cells from heart explants are the following: anti-Neuropilin 1, Abcam ab81321 (1:100); anti-GFP, Roche 11 814 460 001 (1:400); anti-ALDH2, Genetex GTX124302 (1:200); normal rabbit IgG, alpha diagnostics 200009-1-200 (1:400); normal mouse IgG, Invitrogen 026502 (1:400).

The following day, samples were incubated for one hour at room temperature with fluorescent-tagged secondary antibodies (anti-rabbit Alexa 488 and Alexa Fluor 555 Phalloidin, both Thermo Fisher Scientific). Slides were mounted with ProLong DAPI mounting medium (Thermo Fisher Scientific).

Immunoblotting

Lysates were obtained from zebrafish hearts by homogenizing 3 ventricles in RIPA buffer (Sigma-Aldrich) supplemented with TCEP, protease inhibitor cocktail (Roche) and phosphatase inhibitor cocktails (Sigma-Aldrich) in 1.4mm ceramic bead-containing tubes using the Minilys homogenizer (Peqlab). Lysates were supplemented with Lithium dodecyl sulfate anionic detergent (Thermo Fisher Scientific) and RIPA buffer to load equal amount of proteins. All samples were then denatured by heating for 3 minutes at 95°C before loading to gels. Proteins were separated by electrophoresis on 4–12% Bis-Tris polyacrylamide gels, and electrotransferred to PVDF membranes (all Thermo Fisher Scientific). Membranes were blocked with 5% (w/v) non-fat dried milk in PBS containing 0.1% Tween 20 (PBST), incubated with primary antibodies in PBS/blocking solution overnight at 4°C, washed five times in PBST, incubated for 1 hour with horseradish peroxidase-labelled IgG (Santa Cruz biotechnology, Inc.) at room temperature. The antibodies used for immunoblotting are the following: anti-Neuropilin 1, Abcam ab81321; anti-GAPDH V-18, Santa Cruz sc-20357; β actin clone AC-15, Sigma-Aldrich, Cat No. A5441; β catenin, Sigma-Aldrich, Cat No. C2206; all used at 1:100 dilution. Proteins were detected using the ECL Plus™ Western blotting detection system and Hyperfilm (both Amersham).

Recombinant adenovirus generation

All reagents used for the generation of the adenoviruses constructs were from Life Technologies™.

Rat specific NRP1 shRNA construct was generated as previously described (Pellet-Many et al., 2015) using the BLOCK-iT™ U6 RNAi Entry Vector Kit, the primers used to form the hairpins are listed below. The shRNA cassette was recombined into the pAd/BLOCK-iT™-DEST vector and virus produced as described above. The primers used to generate the construct were:

Ad.shNRP1:

5'- CACCGCAGCATCTCTGAAGATTTACGAATGAAATCTTCAGAGATGCTG -3' and,
5'- AAAAGCAGCATCTCTGAAGATTTCAATTCGTGAAATCTTCAGAGATGCTGC -3'

Viral particles were released from the HEK-293A cells by three freeze-thaw cycles and purified using the Adenopure® adenovirus purification kit (Puresyn, Inc.). Purified adenoviruses were dialyzed (Slide-A-Lyzer Dialysis kit: 10,000 MWCO, 2-12 ml capacity, extra strength (Catalogue number 66807) from Thermo Scientific and stored at -20°C until needed.

Epicardial cell NRP1 knock down

Rat Epicardial cells were a generous gift from Dr Nicola Smart and described in (Wada et al., 2003). Cells were tested prior to their use in experiment and were found to be free of mycoplasma. Cells were seeded and left to adhere for 6 to 8 hours. They were then infected with shNRP1 adenovirus constructs for 24 hours as described in Pellet-Many et al. (2015). Protein lysates were harvested and immunoblotting performed as described above.

- GONZALEZ-ROSA, J. M. & MERCADER, N. 2012. Cryoinjury as a myocardial infarction model for the study of cardiac regeneration in the zebrafish. *Nat Protoc*, 7, 782-8.
- KIM, J., RUBIN, N., HUANG, Y., TUAN, T. L. & LIEN, C. L. 2012. In vitro culture of epicardial cells from adult zebrafish heart on a fibrin matrix. *Nature Protocols*, 7, 247-255.
- PELLET-MANY, C., MEHTA, V., FIELDS, L., MAHMOUD, M., LOWE, V., EVANS, I., RUIVO, J. & ZACHARY, I. 2015. Neuropilins 1 and 2 mediate neointimal hyperplasia and re-endothelialization following arterial injury. *Cardiovasc Res*, 108, 288-98.
- WADA, A. M., SMITH, T. K., OSLER, M. E., REESE, D. E. & BADER, D. M. 2003. Epicardial/Mesothelial cell line retains vasculogenic potential of embryonic epicardium. *Circ Res*, 92, 525-31.